Research on Discharge Characteristics of SF_6 Gas with and without Insulator Under Impulse Voltages with Different Waveform Parameters

September 2018

WEN TAO

Title: Research on Discharge Characteristics of SF_6 Gas with and without Insulator Under Impulse Voltages with Different Waveform Parameters

Applicant: WEN TAO

Supervisor: Prof. Naoyuki Shimomura

ABSTRACT

Gas-insulated metal-enclosed switchgear (GIS) may suffer various forms of impulse voltage in operation, including impulses with fast wavefront or short wavetail, and especially very fast transient overvoltage (VFTO), due to the complicated structure of GIS substation. Meanwhile, lightning impulse waveform is widely used in the impulse withstand voltage test to detect the defects in the GIS. The impulse voltage waveform parameters have great influence on the SF_6 discharge characteristics. But the oscillating impulse voltage is often used to study the influence of the wavefront time and the wavetail time parameters on the discharge characteristics. The waveform parameters are complex and have interact influence. Therefore, it is necessary to extract the characteristic parameters of the impulse voltage waveform, and systematically study the effects of single characteristic parameter influence on the discharge characteristics of SF_6 gas with and without insulator.

The platform of SF_6 discharge characteristics under multi-parameter impulses was established in Chapter 2. The experimental platform can generate a double exponential impulse voltage with wavefront time of 0.08 μs ~ 23.5 μs and wavetail time of 1.5 μs to 50 μs, VFTO with single oscillating frequency up to 8.1 MHz and rise time to 49 ns, an oscillating lightning impulse (LI) with wavefront time of 10 μs and oscillating frequency of 25 kHz. A conical voltage sensor was designed to accurately measure MV-level steep pulses with a rise time of less than 7 ns. Different kinds of GIS typical defect structures were used to study the insulation characteristics of SF_6. The 50% discharge voltage was obtained by the up-and-down method.

The discharge characteristics of SF_6 gas under impulse voltages with different waveform parameters, including VFTO, were studied in Chapter 3. The breakdown voltage for VFTO or standard LI in positive polarity is higher than that in negative polarity and the breakdown voltage of VFTO could be lower than that of standard LI at high gas pressure. The breakdown voltage of insulator under VFTO or standard LI in negative polarity is higher than that in positive polarity and the breakdown voltage of defective insulator under VFTO could be lower than that under LI by 8%. The 50% $U_{50\%}$-P curve shows the polarity reversion phenomenon, which can be explained by the migration and diffusion of space charges. The critical pressure of polarity reversion may increase with the increase of electric field inhomogeneity. The impulse

waveform parameters have little influence on the breakdown characteristics of a sound GIS system, but have significant influence on the breakdown characteristics of GIS system with defects. With the rise of gas pressure, the “hump phenomenon” occurs in the $U_{50\%}$-P curves. With the increase of impulse wave front time, the 50% breakdown voltages change significantly and the $U_{50\%}$-T_f curves tend to be U-shaped. The bigger the electric field factor f is, the more obvious the U-shaped trend is. The 50% breakdown voltages decrease significantly with the increase of impulse wave tail time. When the wavetail time increases, the discharge voltage gradually decreases, which could be explained by the area method.

The discharge characteristics of SF_6 gas under impulse votlages with wide range wavefront time were studied in Chapter 4. The insulation defects detecting effectiveness of oscillating LI with long T_f around 10 μs is lower than that of standard LI. According to the voltage-time characteristic, it can be inferred that the T_f plays an important role in the insulation defect detecting effectiveness. With T_f increases, the 50% breakdown voltages for rod-plane gaps have an increased trend. The V-t curves of rod-plane gap under short T_f and long T_f present an opposite trend. The V-t curve shows a U-shaped in a wide range of t_b. The gap distance (or field nonuniformity factor) influences the shape of V-t curve. With the gap distance increase, the flat part of the curve and the mouth of the U-shaped V-t curve become narrower. The 50% flashover voltage of the insulator with surface conductive defects increases with the increase of wavefront time, which is similiar with the results of gas gap. The effect of T_f is the effect of the slope of impulse dU/dt essentially. SF_6 gaps with a higher field nonuniformity factor f are more sensitive to dU/dt, also to T_f. Corona stabilization effect is not just in relationship with the rise rate of impulse, but also with electrode structure and gas pressure. The critical dU/dt for corona stabilization is calculated for different rod-plane gaps.

The effect of electrode structure on discharge characteristics was researched in Chapter 5. The electrode structure has a great influence on the discharge characteristics. For the GIS bus with a conductive protrusion, the shielding effect of the bus on the defect changes the electric field distribution of the gap, so that the $U_{50\%}$-T_f curves no longer show the U-shaped as the rod-plane electrode. The 50% discharge voltage of the bus with needle increases with wavefront time increase. The field simulation results also show that with the increase of the needle length, the field nonuniformity factor increases.

The on-site standard lightning impulse test technology was studied in Chapter 6. A new fully enclosed and compact standard LI generator with low inductance has been developed, using SF_6 gas as the insulating medium and incorporating novel structural design of the switch capacitor integration unit. Using the developed generator, an on-site standard LI test for 1100 kV GIS was successfully carried out in a UHV

substation. One circuit breaker and its accessories were connected as the load for each test.

KEY WORDS: Gas-insulated metal-enclosed switchgear (GIS); Very Fast Transient Overvoltages (VFTO); SF_6; Impulse Test; Wavefront Time; Wavetail time; Discharege Characteristic.

CONTENTS

CHAPTER 1. PREFACE

1.1 Introduction

Gas-insulated metal-enclosed switchgear (GIS) has been developed rapidly since the mid-1960s [1-5]. Compared with traditional air insulated switchgear, the GIS makes the bus, disconnector switch, circuit breaker, lightning arrester, and many other devices all concentrated in an enclosed grounding metal case. So it has many advantages such as reliability, compaction, long maintenance cycle, and small impact on the environment, widely used today in electrical power systems [6-16]. The typical connection mode of the GIS used in power substation is shown in Figure 1-1.

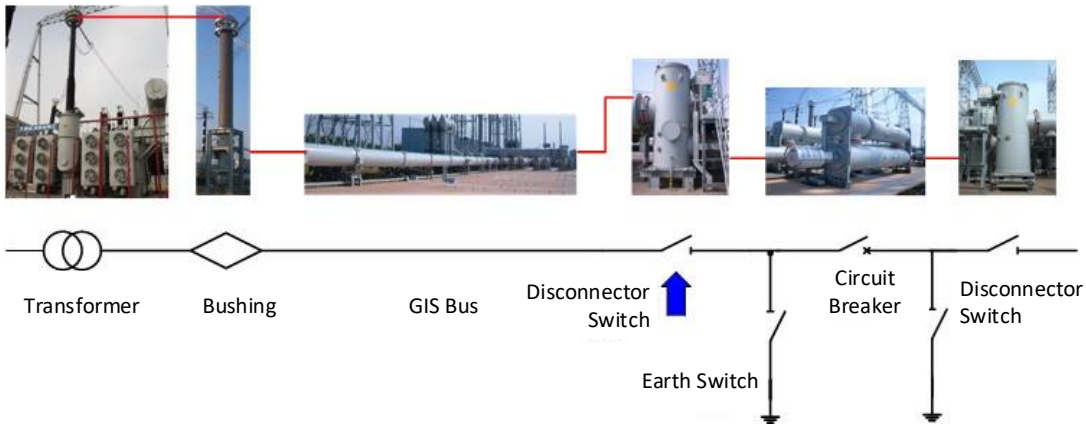

Figure 1-1. Typical connection mode of the GIS used in power substation

With the increase of voltage grade, the importance of electric power equipment such as GIS, the significance, failure rate, maintenance cost, and capacitance are further improved. At the same time, the GIS insulation defects caused by design, processing and on-site installation, would lead to insulation breakdown in the process of operation [17-18]. Along with the development of the power grid, more and more insulation breakdown accidents caused by the internal insulation defects of GIS appear, which have great influence on the power system safe and reliable operation.

Nowadays, gas-insulated metal-enclosed switchgear (GIS) has been developed rapidly and widely used in power system. More steep impulses would appear due to the reflection or deformation in the GIS. In addition, very fast transient overvoltages (VFTOs) [19-21], coming from the normal operation of a disconnector, have a fast rise time ranging from 3 to 100 ns, which would cause much more insulation failures, as shown in Figure 1-2. Impulses with fast rise time less than 1.2 μs should be considered and insulation strength under these impulses should attract the attention of researchers.

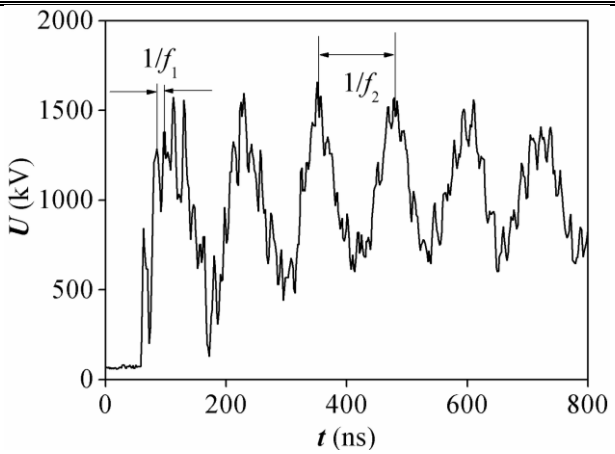

Figure 1-2. VFTO caused by disconnector switch operation in a 1100 kV GIS

Moreover, in order to obtain the insulation characteristics under impulses or surges, the impluse tests are carried out in the type test, factory test and on-site test. During the test, the test impulse waveforms are various because of the test purpose or the circuit parameters. Usually, lightning impulse (LI) test is widely used in these situations. LI test is particularly sensitive to detect abnormal electric field structure, such as the electrode damage [22], as shown in Table 1-1.

Table 1-1. Relative effectiveness of on-site test on GIS defect [22]

Defect	On-site Testing				
	High AC without PD	Low AC with PD	High AC with PD	Lightning Impulse	Switching Impulse
Protrusions on HV electrodes			Δ	○	Δ
Particles, tracks on spacers			○	○	Δ
Cracks, burrs inside spacers	Δ	Δ	○	Δ	Δ
Free particles	○	○	○		Δ
Part floating	Δ	○	○		
Left foreign bodies	○	Δ	○	○	Δ

○ Effective Δ Less Effective

LI test is proposed for the first time by Philip Sporn in 1928 [23-24]. Before this, AC voltage is the mean method to measure the insulation strength, guide the equipment design, production and installation. After several years' discussion, based on the observation of lightning surges in the actual field, the standard LI waveform is introduced to the IEC standard in 1962. In this standard, the standard LI voltage is defined as follows: "The standard lightning impulse voltage is a smooth full lightning impulse voltage having a front time of 1.2 μs and a time to half-value of 50 μs", namely 1.2/50 μs [25]. The wavefront time is calculated by "30 ~ 90% method". These values have remained unchanged from IEC Ed. 1 in 1962 through to Ed. 3 in 2010. During the discussion of standard LI waveform, different waveforms with

wavefront time less than 1.2 μs, such as 0.25, 0.5 μs, and wavetail time less than 50 μs, such as 10, 30 μs, have also been proposed based on years of observation [24]. For the difficulty in generating a lightning-impulse waveform with steep front time due to factors such as the series inductance attributable to the test circuit and the capacitance of the equipment to be tested, the steep wavefront time less than 1 μs was revised to 1 μs and latterly to 1.2 μs [26].

With the increase of voltage grade, the capacitance of power equipment is large, especially for EHV and UHV GIS and long gas insulated line (GIL) equipment. The standard LI waveform is also difficulty to be generated. The IEC has also proposed a non-standard LI test in which the T_f of the impulse voltage waveform can be as much as 8 μs, or, when using oscillating LI voltages, as much as 15 μs [27]. Hence, the insulation characteristics under non-standard LI should be studied.

1.2 Research Status

At present, although a large number of scholars at home and abroad have carried out research on the insulation characteristics of SF_6 under impulse voltage [28-34], the systematic study of the impulse voltage waveform parameters has less influence on the discharge characteristics, and the voltage waveforms used in the experimental is not uniform. So the results has large data dispersion and poorly comparable. This section mainly reviews the research status of the basic characteristic parameters of the impulse voltage waveform, namely the wavefront time and the wavetail time on the SF_6 gas discharge characteristics.

1.2.1 Influence of Impulse Wavefront Time on Discharge Characteristics

It is well known that GIS generally uses a quasi-uniform electric field structure such as a coaxial cylinder or a concentric sphere. A lot of basic researches on the discharge characteristics of this electric field structure under the impulse voltage with different waveform parameters have been carried out at home and abroad [30-32]. And a more consistent conclusion is obtained, that is, the impulse voltage wavefront time has little effect on the discharge voltage of quasi-uniform electric field SF_6 gas gap. Although the GIS structure is quasi-uniform electric field in the macroscopic view, in the intermediate process of actual machining, assembly, transportation, etc., metal conductive particles are inevitably left inside, and local electric field concentration is formed, which causes the SF_6 gas breakdown electric field strength to drop drastically. These residual metal particles, burrs and sharp corners on the surface of the GIS bus are ubiquitous in GIS, and are practically inevitable. G. Luxa et al. give the breakdown voltage-breakdown dely time (V-t) characteristic curve of SF_6 gap breakdown under VFTO and LI, as shown in Figure 1-3 [35]. It can be seen from Figure 1-3 that for a highly inhomogeneous electric field, the V-t curve of the SF_6 gap breakdown voltage increases as the breakdown delay increases. For the curve undr VFTO with extremely steep wavefront time, the V-t curve is below the others'. The breakdown delay time is related to the impulse wavefront time. Therefore, it can be

explained that the impulse voltage wavefront time has a significant effect on the discharge characteristics of SF_6 highly inhomogeneous electric field. However, this study only gives the relationship of the V-t curve with the breakdown delay time qualitatively.

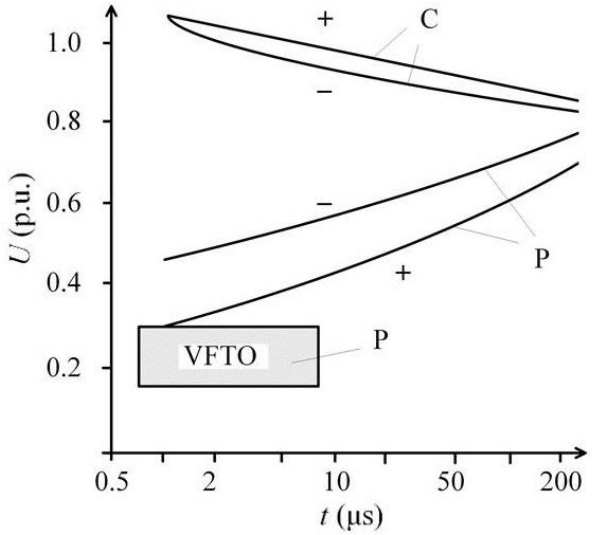

C：Coaxial gap　P：needle-plane gap

Figure 1-3.　Relative breakdown voltage and breakdown delay [35]

S. Matsumoto et al. studied the positive impulse breakdown characteristics of coaxial cylindrical electrode structures for a high voltage conductor attached metal needles [36]. The experiment used oscillating impulse voltages with wavefront time of 0.24 μs, 2.3 μs, 8.3 μs, 33 μs, 59 μs, 186 μs, 250 μs and 306 μs respectively. The V-t cureves has a wide range of breakdown delay time, as shown in Figure 1-4. The results show that the defect size in GIS affects its sensitivity to the impulse wavefront time. As the size of the metal particles decreases, the discharge voltage increases fastly with the wavefront time. The longer the length of the needle is, the more inhomogeneous the electric field is, and the U-shape appears in the V-t curve. As the breakdown delay time increases, the V-t curve first drops, and then goes up after a relatively flat area. The higher the pressure, the more obvious the U-shaped trend. The conclusion of the U-shaped right half-up is consistent with the G. Luxa study, but the critical breakdown delay time is different. S. Okabe et al. found that the V-t curve has a small change in discharge voltage in the region of 1.0 μs ~ 10 μs according to Figure 1-4(b). It is considered that when there is local electric field concentration in the GIS, the LI withstand voltage test wavefront time can be relaxed. The upper limit of time to 3.6 μs has no effect on the effectiveness of the impulse test [28]. But the flat area has fewer data points and does not effectively support the conclusion of 3.6 μs. To some extent, the V-t characteristic curve can reflect the relationship between the wavefront time and the discharge voltage, but the range of the breakdown delay time of the V-t curve corresponding to the flat region is not equal to the wavefront time of the impulse voltage. In addition, the above research does not distinguish the data under

different wavefront time impulse voltages, and can not accurately obtain the influence of the impulse voltage wavefront time on the discharge characteristics.

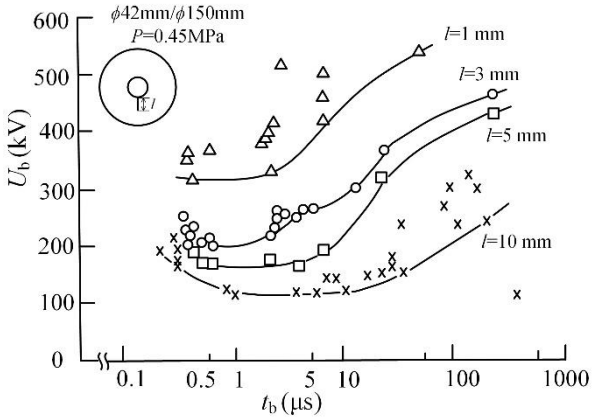

(a) different needle length, positive polarity

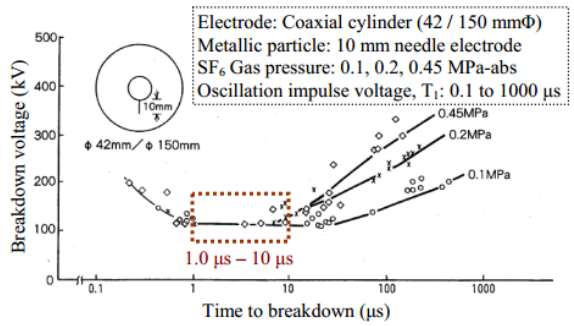

(b) different gas pressure, positive polarity

Figure 1-4. V-t characteristic of a coaxial cylinder arrangement with metallic particles [36]

In paper [37], the discharge characteristics of the SF_6 gas gap of the highly inhomogeneous electric field under impulses with high oscillating frequency are studied. The standard values of the gap discharge voltages under different wave tail time constants τ are obtained as shown in Figure 1-5.

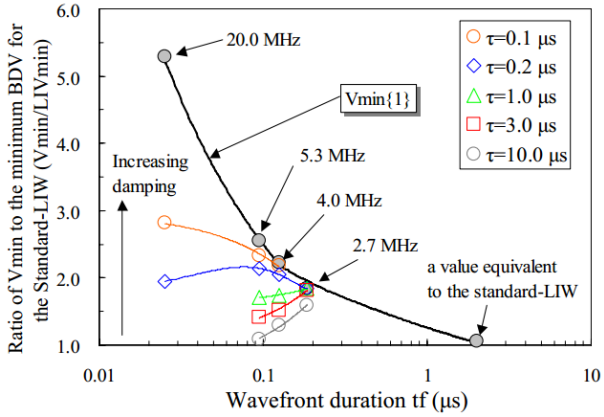

Figure 1-5 Characteristics of minimum breakdown voltages (Vmin/LIVmin) at diverse frequencies obtained while changing the wave front duration [37]

The results show that the wavefront time is in the range of tens of ns to hundreds of

ns, when the value of τ is large, the gap discharge voltage increases with the increase of the wavefront time. When the τ decreases to a certain value, the gap discharge voltage decreases with the wavefront time increases, indicating that the oscillating time constant of the wave tail will affect the variation of the gap discharge voltage with the wavefront time. Most of the above studies use oscillating impulse voltage, and the waveform parameters are more complicated. The law obtained can not accurately reflect the influence of wavefront time on the discharge characteristics.

Some other researchers have tried to explain the reason of VFTO insulation accidents by studying the SF_6 gas gap discharge characteristics under the steep fronted impulse voltage of the wavefront time range of 50 ns ~ 1.2 μs [38]. The study uses 50% breakdown voltage to measure the difference of discharge characteristics under different wavefront impulse voltages, which indicates that the impulse voltage wavefront time has a significant effect on the breakdown voltage of SF_6 gas in the highly inhomogeneous field. The relationship of breakdown voltage U_b and the wavefront time T_f shows a concave U-shaped curve, as shown in Figure 1-6. However, the study uses a narrow wavefront time range and does not reflect the discharge characteristics at a impulse voltage with a longer wavefront time range. In addition, S. Matsumoto et al.'s research also shows that the sensitivity of the discharge characteristics to the wavefront time is related to the electrode structure parameters. Therefore, it is necessary to further systematically study the discharge characteristics of different electrode structures under a single variable of a wide range of wavefront time.

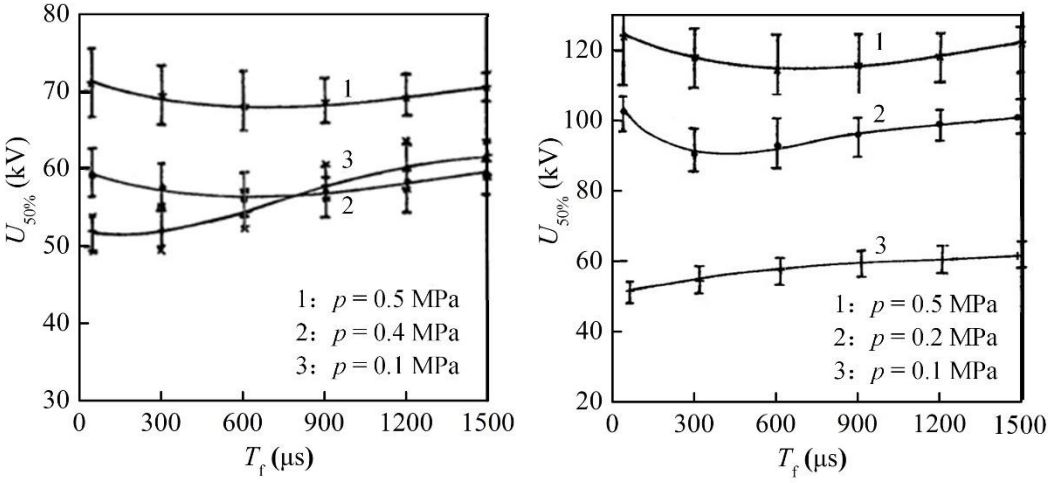

(a) positive polarity (b) negative polarity

Figure 1-6. 50% breakdown voltage vs. wavefront time for 10 mm needle-plane gap [38]

1.2.2 Influence of Impulse Wavetail Time on Discharge Characteristics

Some scholars used the impulse voltage wavetail time (half-peak time) to characterize the voltage damping time. The relationship between the discharge voltage of the needle-plane electrode and the gas pressure under the steep wavefront impulse voltage of different tail time was studied. It is considered that when the wavetail time is increased from 50 μs to 550 μs, the discharge voltage has only a small change [38],

as shown in Figure 1-7. However, the variation range of the wavetail parameters in this experiment is too broad, the needle-plane electrode gap is short, and the discharge delay time is only a few μs. When discharge, the wavetail voltage drops less, so the discharge voltage difference is small. The actual wavetail of surges and VFTO tend to decay faster. Therefore, it is necessary to systematically study the discharge characteristics of SF_6 gas under the impulse voltage with fast wavetail attenuation.

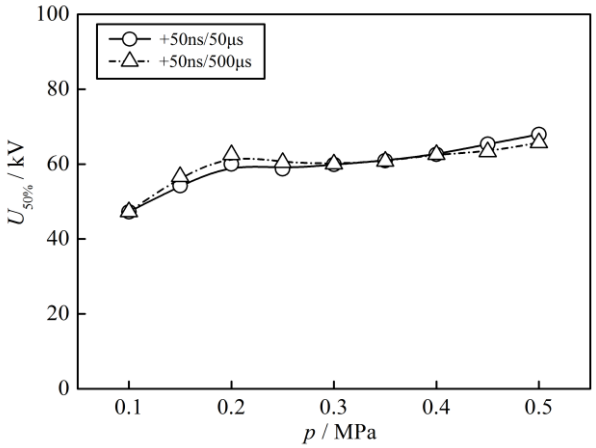

Figure 1-7. Effect of wavetail time on the discharge characteristics of needle-plane gap [38]

It can be seen from the existing research results that on the one hand, the impulse voltage waveform parameters have a great influence on the SF_6 discharge characteristics. But the oscillating impulse voltage is often used to study the influence of the wavefront time and the wavetail time parameters on the discharge characteristics. The waveform parameters are complex and have interact influence. On the other hand, the influence of the impulse voltage waveform parameters on the discharge characteristics is also related to the electrode structure and the electric field non-uniformity coefficient. However, the current study adopts a single electrode structure, which can only qualitatively reflect the influence law. Therefore, it is necessary to extract the characteristic parameters of the impulse voltage waveform, and systematically study the effects of single characteristic parameter influence on the discharge characteristics of SF_6 gas under different electrode structures and electric field inhomogeneity coefficients.

1.3 Major Research Content of the Paper

It can be seen from the existing research results that on the one hand, the impulse voltage waveform parameters have a great influence on the SF_6 discharge characteristics. But the oscillating impulse voltage is often used to study the influence of the wavefront time and the wavetail time parameters on the discharge characteristics. The waveform parameters are complex and have interact influence. On the other hand, the influence of the impulse voltage waveform parameters on the discharge characteristics is also related to the electrode structure and the electric field non-uniformity coefficient. However, the current study adopts a single electrode

structure, which can only qualitatively reflect the influence law. Therefore, it is necessary to extract the characteristic parameters of the impulse voltage waveform, and systematically study the effects of single characteristic parameter influence on the discharge characteristics of SF_6 gas under different electrode structures and electric field inhomogeneity coefficients.

The major research content of the paper is as follows:

1) Research on the platform of SF_6 discharge characteristics under multi-parameter impulses.
2) Research on the discharge characteristics of SF_6 gas under impulse votlages with different wavefrom parameters.
3) Research on the discharge characteristics of SF_6 gas under impulse votlages with wide range wavefront time.
4) Research on the effect of electrode structure on discharge characteristics.
5) Research on the on-site standard lightning impulse test technology.

CHAPTER 2. RESEARCH PLATFORM OF SF_6 DISCHARGE CHARACTERISTICS UNDER MULTI-PARAMETER IMPULSES

In order to obtain the discharge characteristics of SF_6 gas with and without insulator under impulse voltages with different waveform parameters, based on the fully enclosed, oil-immersed impulse generator,. the platform of SF_6 discharge characteristics under multi-parameter impulses was established. The platform can generate a double exponential LI with a wavefront time of 0.08 μs ~ 23.5 μs, a tail time of 1.5 μs ~ 50 μs, a VFTO with a rising edge of several tens of ns and oscillating LI with long wavefront time. The waveform parameters can be easily adjusted by the centralized wavefront resistance and the wavetail resistance.

2.1 Generation and Measurement of Multi - parameter Impulses

2.1.1 Generation of Multi - parameter Impulses

A multiple parameters impulse generating system based on a fully enclosed, oil-insulated Marx generator and a simulated GIS bus is established, as shown in Figure 2-1. The Marx generator and simulated GIS bus are separated by dielectric spacers and a basin-type insulator. By immersing the Marx generator in oil, it can be made very compact, thereby lowering inductance, which affects the front time of the output wave. The generator could generate LI with wavefront time (T_f) in the range of 0.08 to 23.5 μs and wavetail time (T_t) in the range of 1.5 to 46.5 μs (including standard LI, 1.2/46.5 μs, within the error range), as shown in Figure 2-2. In order to avoid other influence on the experiment results, the wavetail time was fixed at 46.5 μs when studying the effect of wavefront time for the wavetail time was long enough compared with wavefront time. And the wavefront time was fixed at 0.08 μs in the study of wavetail time effect for the breakdowns would almost happen in the wavetail of these impulses.

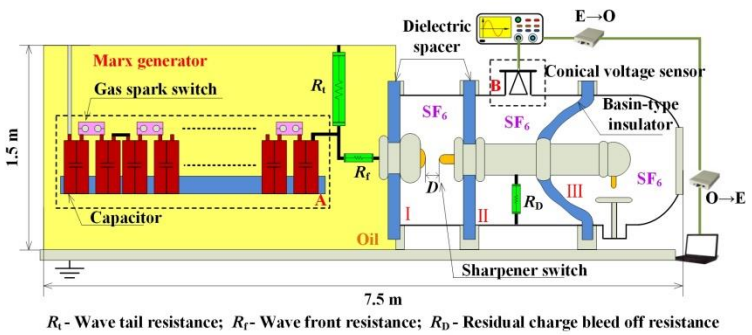

Figure 2-1. Schematic diagram of multiple parameter impulses generating system

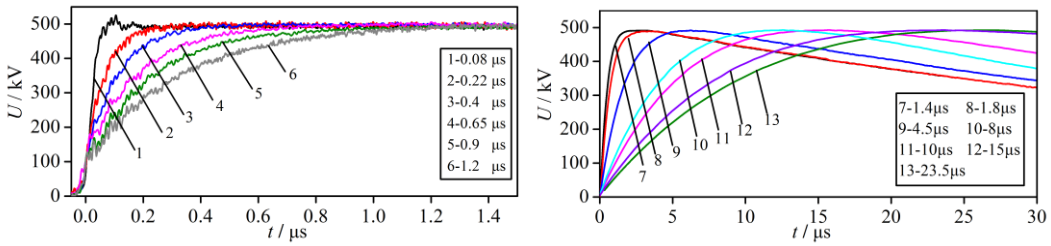

(a) LI with different wavefront times (T_f = 0.08 μs ~ 23.5 μs, T_t = 46.5 μs)

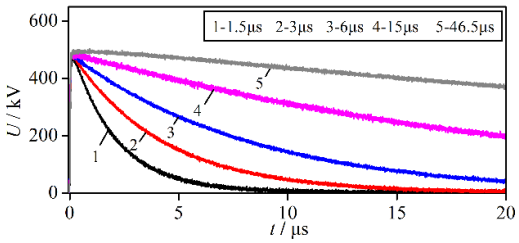

(b) LI with different wavetail times (T_f = 0.08 μs μs, T_t = 1.5 μs ~ 46.5 μs)

Figure 2-2. Output LI with different waveform parameters

The generator could generate VFTO with single frequency oscillating up to 8.1 MHz shown in Figure 2-3. Front time of the first wave T_f, wave tail time T_t, oscillation frequency f and oscillating coefficient ξ were the four major parameters of VFTO. Oscillating coefficient was proposed to clarify the wave oscillation amplitude. ξ here is defined as:

$$\xi = \frac{(V_1 - V_2)/2}{V_1 - (V_1 - V_2)/2} \tag{2-1}$$

Where, V_1 and V_2 are the first peak value and the first trough value of the VFTO respectively.

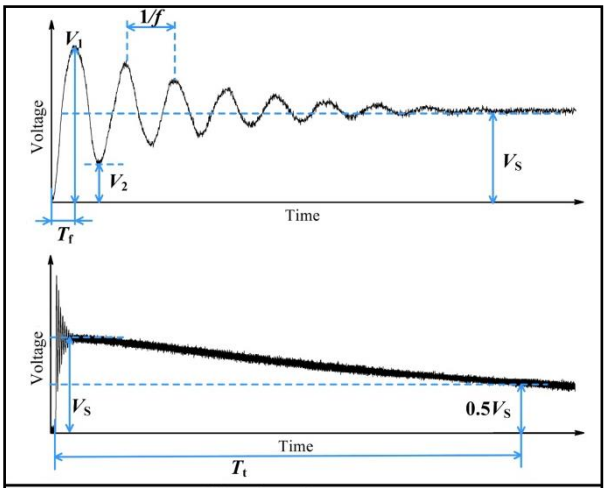

Waveform Parameters			
T_f	T_t	f	ξ
49 ns	46.57 μs	8.1 MHz	0.35~0.8

Figure 2-3. Typical voltage waveform of VFTO

Meanwhile, an oscillating LI (OLI) with wavefront time around 10 μs and oscillation frequency around 25 kHz, as shown in Figure 2-4.

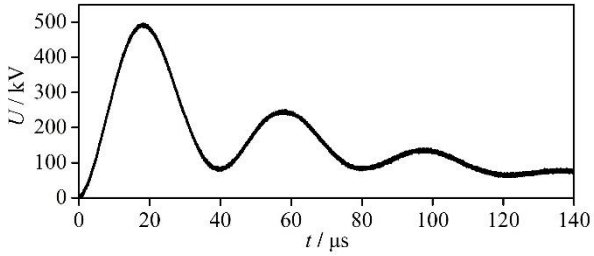

Figure 2-4. OLI with T_f around 10 μs

2.1.2 Measurement of Multi - parameter Impulses

The amplitude of test voltage to be measured is several megavolts, which requires a large voltage attenuation ratio of the voltage sensor. A conical voltage sensor is installed into the reserving window of Cavity II in Figure 2-1**,** as shown in Figure 2-5. A polyimide film (PI) with a few microns thick between the inner and outer aluminum cones is the dielectric of the low-voltage arm (C_2). The low-voltage arm's capacitance of the conical voltage sensor is higher than that of a traditional plane voltage sensor, so the voltage attenuation ratio is larger when the sensor electrode has the same size. In addition, the conical structure of the voltage sensor can make the wave impedance translate smoothly from the high-voltage arm (C_1) to the coaxial cable, which significantly reduces refraction and reflection of the voltage wave when it propagates in the measurement system. The fast front time calibrating result and long wave tail calibrating result indicate that the response of the newly developed conical voltage senor is less than 7 ns and it could also satisfy the measuring requirement of the impulse with wave tail around 150 μs accurately.

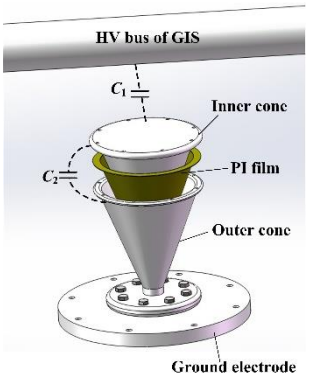

Figure. 2-5 Sketch of the conical voltage sensor

A standard water resistor voltage divider was used for the calibration of the conical voltage sensor. Figure 2-6 compares the results of both types of voltage measurements under a very fast rise time waveform. The front time of the impulse measured by standard water resistor voltage divider and conical voltage sensor were 6.35 ns and 6.92 ns, respectively. This shows that the newly developed conical voltage sensor accurately measures the fast front time impulse and has a stable voltage attenuation ratio. The long wave tail calibrating result of the conical voltage sensor is shown in Figure 2-7. The tail of the wave measured by the standard resistance voltage divider

was 148 μs whereas the conical voltage sensor was 151 μs. This demonstrates that the newly developed conical voltage sensor can accurately measure the 50 μs tail of a standard LI.

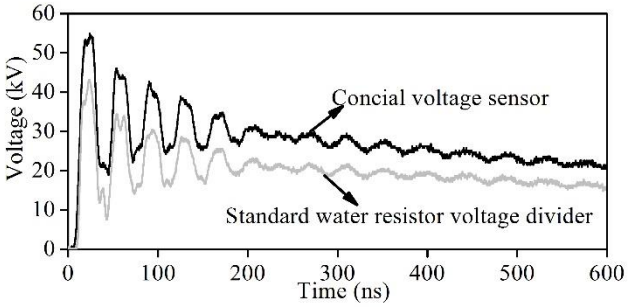

Figure 2-6. Comparison of response to a very fast rise time waveform of a standard water resistor voltage divider and conical voltage sensor

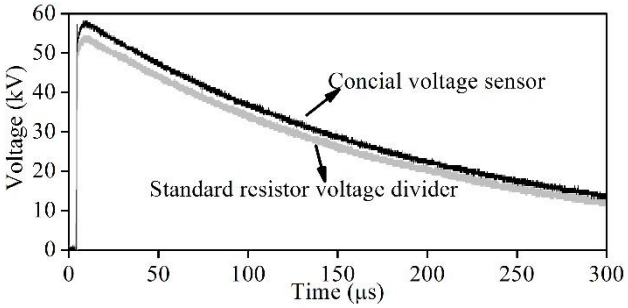

Figure 2-7. Long wave tail calibrating result of the conical voltage sensor

2.2 Simulation of GIS Typical Insulation Structures

2.2.1 SF_6 Gas gap without insulator

The rod-plane electrode and sphere-plane electrode shown in Figure 2-8 were used to simulate slightly inhomogeneous coaxial field. The high voltage electrode in Figure 2-8(a) was a hemispherically capped stainless steel rod with different curve radius *r*. The high voltage electrode in Figure 2-8(b) was a 150-mm-radius sphere made of stainless steel. The grounded plane was a 300-mm-diam Rogowski stainless steel electrode. The electrode gap d could be adjusted in the test. The electrodes parameters used in this paper were shown in Table 2-1. The test setups were installed in the chamber filled with SF_6 up to absolute pressures ranging from 0.1 to 0.6 MPa.

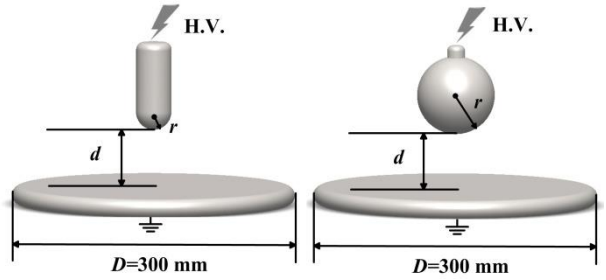

(a) rod-plane (b) sphere -plane

Figure 2-8. Configuration of rod-plane electrode

Table 1. Electrodes parameters of rod-plane electrodes

Parameters	Rod-plane								Sphere -plane
r/mm	15	15	8	2	1	0.5	0.5	0.5	150
d/mm	15	33	112	33	33	33	45	60	72

However, for GIS, the defects may occur in the high voltage bus. In this situation, it's not just the rod-plane electrode can be represented. In this paper, in order to research the shielding effect of background electric field for GIS bus with a conductive protrusion under impulses, a special test electrode was designed, as shown in Figure 2-9. In the test electrode, the high voltage electrode was a GIS bus with a conductive protrusion. The diameter of the bus was 72 mm. The conductive protrusion was a needle with a diameter of hundreds of μm. The needle was perpendicular to the bus surface and the length of it (*L*) could be adjusted form 3 mm to 40 mm. The ground electrode was a 300-mm-diam Rogowski stainless plane. The distance from the tip of the needle to the plane was fixed to be 33 mm by the adjusting the plane.

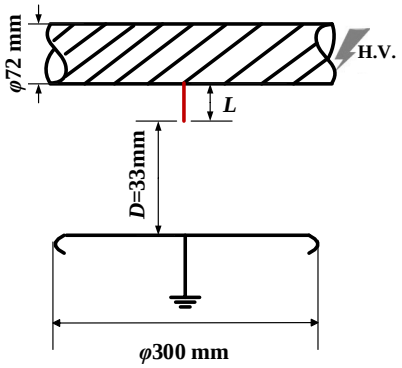

Figure 2-9. Coaxial cylinder structure with protrusion

Coaxial cylinder structure of 126 kV class (φ_1/φ_2 = 72/230 mm), 252 kV class (φ_1/φ_2 = 72/320 mm), 550 kV class (φ_1/φ_2 = 170/550 mm) with conductive protrusion were used to simulate the practical defect, as shown in Figure 2-10. The conductive protrusion was a r = 0.5 mm rod or a needle with tens of micrometer. The length of the protrusion was 3, 5, 10 mm.

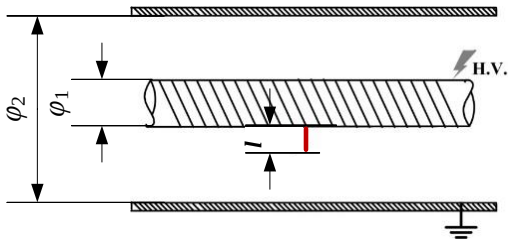

Figure 2-10. Electrode configuration of coaxial cylinder structure with conductive protrusion

2.2.2 SF_6 Gas gap with insulator

A 550 kV GIS basin-type insulator was used in this paper. The high voltage electrode in Figure 2-11was a 75-mm-radius cylinder. The inner radius of the

grounded cylinder was 277 mm. A steel needle with a length of 15 mm was attached to the insulator surface. The needle was 0.5 mm in diameter with a point tip radius of 0.1 mm. Care was taken to ensure that both ends of the particle were not covered with adhesive. The position of the needle on insulator could be adjusted.

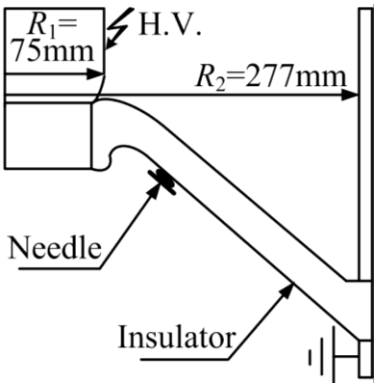

Figure 2-11. Metal-contaminated basin-type insulator (550 kV)

The 126 kV basin-type insulator with coaxial cylindrical electrode structure was used as the research object to research the influence of impulse waveform parameters on the flashover voltages, as shown in Figure 2-12. The diameter of the steel needle was 0.56 mm and the length was 8 mm, and it was attached to the surface of the insulator near the high voltage conductor side. At the same time, the 126 kV post insulator with needle defect was also used. The diameter of the steel needle was 0.56 mm and the length was 4 mm, as shown in Figure 2-13.

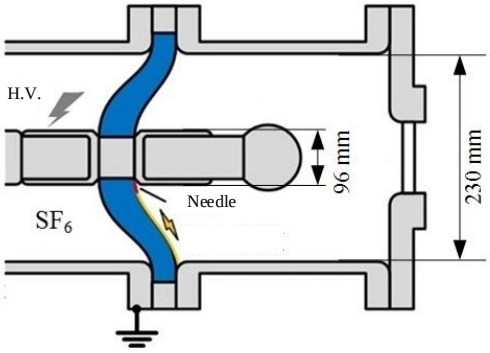

Figure 2-12. Metal-contaminated basin-type insulator (126 kV)

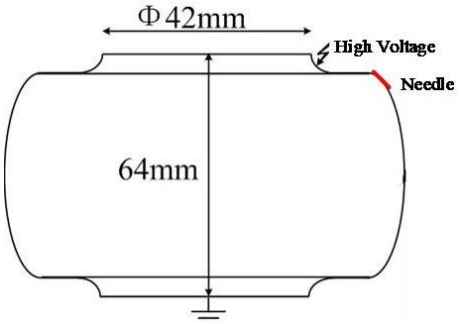

Figure 2-13. Post insulator with conductive particle attached to its surface (126 kV)

2.3 Experimental Method

In SF_6 highly inhomogeneous electric field, the breakdown voltage under positive polarity is lower than that under negative polarity. So the positive polarity voltage was used in this study. The waveforms were recorded using an oscilloscope (Tektronix DPO4104) with a bandwidth of 1 GHz and a sample rate of 5 Gs/s. Calibration results demonstrated that the response time of the measuring system was less than 5 ns and the uncertainty of divider ratio was less than 3%. The voltage-time characteristic of the rod-plane electrode system was obtained by applying impulse voltages of various amplitudes, and its 50% breakdown voltage by using the up-and-down method described in IEC 60060-1.

Here, the prospective voltage value used in the calculation of 50% breakdown voltage, and the breakdown voltage value used in the voltage-time characteristic, should be clarified, which maybe cause some misunderstandings in the follow discussions of insulation defect detecting effectiveness. The 50% breakdown voltage is the prospective voltage value which has a 50% probability of producing a disruptive discharge on the test object. When calculating the 50% breakdown voltage (equal the mean value of the data obtained using up-and-down method), it should use the prospective voltage value, not the recorded breakdown voltage values.

For the used impulse waveforms, the breakdown may occur in the front, near the peak, or in the tail of the impulse. For breakdown occurs in the front of the impulse (breakdown time $T_b < T_f$), as shown in Figure 2-14(a), the breakdown voltage is the peak value of the recorded waveform (If breakdown, the impulse will fast drop to zero from the breakdown point and the part after breakdown point cannot be recorded). But the prospective voltage is the peak value of the full waveform assumed that the test object is not breakdown. In this case, the prospective voltage is higher than the breakdown voltage. For breakdown occurs near the peak or in the tail of the impulse (breakdown time $T_b \geq T_f$), as shown in Figure 2-14(b), the breakdown voltage is the peak value of the recorded waveform as well. In this case, the prospective voltage is equal to the breakdown voltage. The insulation defect detecting effectiveness using the impulse test is reflected in the value of the prospective voltage, i.e., the higher the prospective voltage the lower the effectiveness of defect detection.

The prospective voltage value U_p, not affected by the measured waveform, is the peak value of the impulse voltage stressed on the test object assumed that there is no disruptive discharge, calculated by the impulse voltage generator's charging level voltage U_L, levels N and output efficiency η ($U = U_L \cdot N \cdot \eta$). The double-exponential impulse's waveform function can be written as follows.

$$U(t) = U_m(e^{-at} - e^{-bt}) \tag{2-2}$$

Where, U_m is the amplitude parameter, equals to The prospective voltage value U_p. a, b are waveform parameters, considered by the wave tail time and wavefront time respectively. When the breakdown time T_b and the breakdown voltage U_b are known,

the prospective voltage value *U* can also be calculated by the stressed waveform function *U*(t).

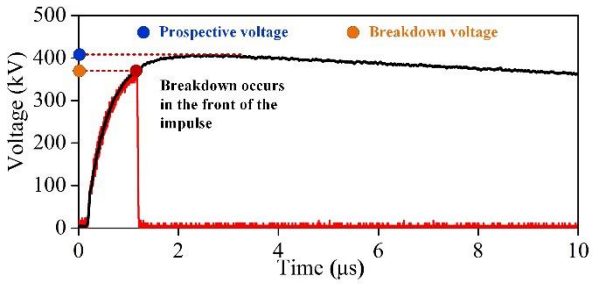

(a) breakdown occurs in the front

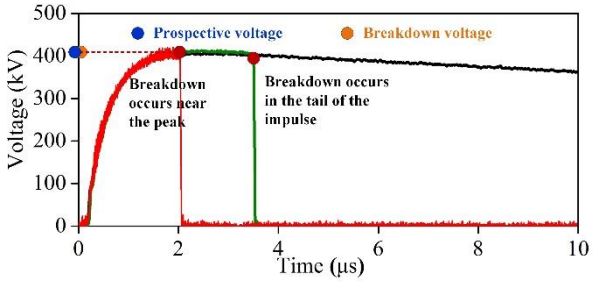

(b) breakdown occurs near the peak or in the tail

Figure 2-14. Definition of the prospective voltage and breakdown voltage in the article

2.4 Brief Summary

The platform of SF_6 discharge characteristics under multi-parameter impulses. was established. The experimental platform can generate a double exponential impulse voltage with wavefront time of 0.08 μs ~ 23.5 μs and wavetail time of 1.5 μs to 50 μs, VFTO with single oscillating frequency up to 8.1 MHz and rise time to 49 ns, an oscillating LI with wavefront time of 10 μs and oscillating frequency of 25 kHz. A conical voltage sensor was designed to accurately measure MV-level steep pulses with a rise time of less than 7 ns. Different kinds of GIS typical defect structures were used to study the insulation characteristics of SF_6. The 50% discharge voltage was obtained by the up-and-down method.

CHAPTER 3. DISCHARGE CHARACTERISTICS OF SF_6 GAS UNDER IMPULSE VOLTAGES WITH DIFFERENT WAVEFORM PARAMETERS

GIS may suffer various forms of surge in operation, including surges with fast wavefront or short wavetail, and especially VFTO, due to the complicated structure of GIS substation. In order to obtain the insulation characteristics under these impulses, in this chapter, first, the discharge characteristics of SF_6 under VFTO were studied. Then the wavefront time 0.08 μs ~ 1.2 μs and wavetail time 1.5 μs ~ 46.5 μs were selected as the typical parameters to study the influence of waveform parameters.

3.1 Discharge characteristics of SF_6 gas under VFTO

3.1.1 Discharge Characteristics of SF_6 Gas Without Insulator

For a non-uniform field, typically the rod-plane gap, the breakdown voltage is usually observed to be lower when the rod electrode is biased positively [39, 40], whereas the polarity effect for the rod-plane gap in this thesis has been found to be different. Figure 3-1 shows the breakdown voltage of SF_6 gas as a function of pressure under different voltage polarities. In positive polarity, the 50% breakdown voltage is higher than that in negative polarity for both VFTO and standard LI. Interestingly, at 0.5 MPa the 50% breakdown voltage under VFTO could be is lower than that under standard LI for the negative polarity. In other words, VFTO with negative polarity is a bigger threat to the insulation of GIS than standard LI. The ξ of VFTO stressed on the rod-plane electrodes and insulator was 0.35.

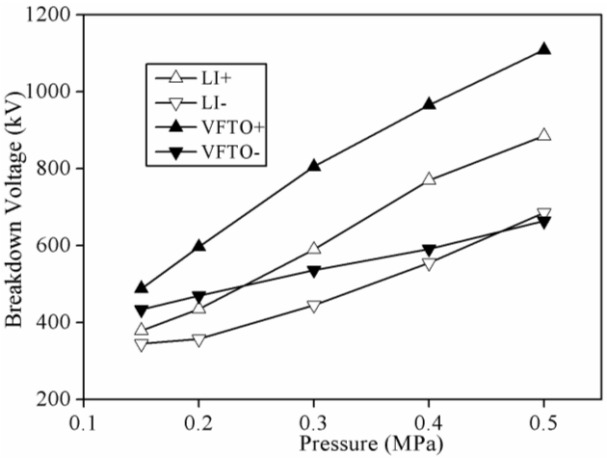

Figure 3-1. Breakdown voltage vs. gas pressure for 112 mm rod-plane gap

Figure 3-2 shows the *V-t* curves of the rod-plane gap under VFTO and LI at

different pressures. It can be seen from Figure 3-2(a) that the *V-t* curves of VFTO and standard LI intersect for positive or negative polarity at a lower pressure. Similarly, at higher pressure the *V-t* curve of VFTO for negative polarity falls below that of standard LI, as shown in Figure 3-2(b).

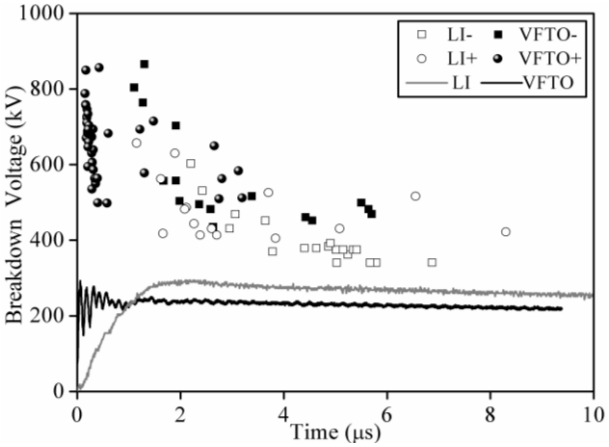

(a) p = 0.2 MPa

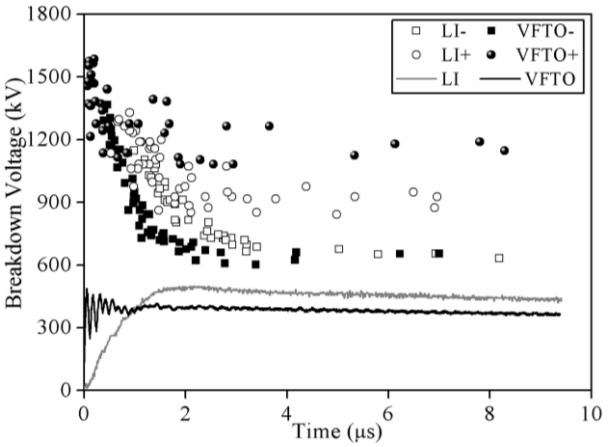

(b) p = 0.5 MPa

Figure 3-2. V-t curves of rod-plane gap under VFTO and LI (d=112 mm)

3.1.2 Discharge Characteristics of SF_6 Gas With Insulator

The breakdown voltage of insulator with and without defects is shown in Figure 3-3 and the corresponding discharge images are shown in Figure 3-4. The length x is defined as the distance between inner electrode and the needle. The insulator without defect is represented by x=0.

Corona stabilization effect is lost in quasi-uniform electric field. Thus, the breakdown voltage of insulator without defect under VFTO or LI in positive polarity is higher than that in negative polarity. When the insulator is contaminated by a needle, the breakdown process contains two steps, i.e. the breakdown between inner electrode and the needle as well as the breakdown between the needle and outer electrode. In Fig.3-4(b), partial arc bridges the inner electrode and needle at first. The electric field in front of needle is non-uniform, resulting the breakdown voltage for VFTO or LI in positive polarity is lower than that in negative polarity.

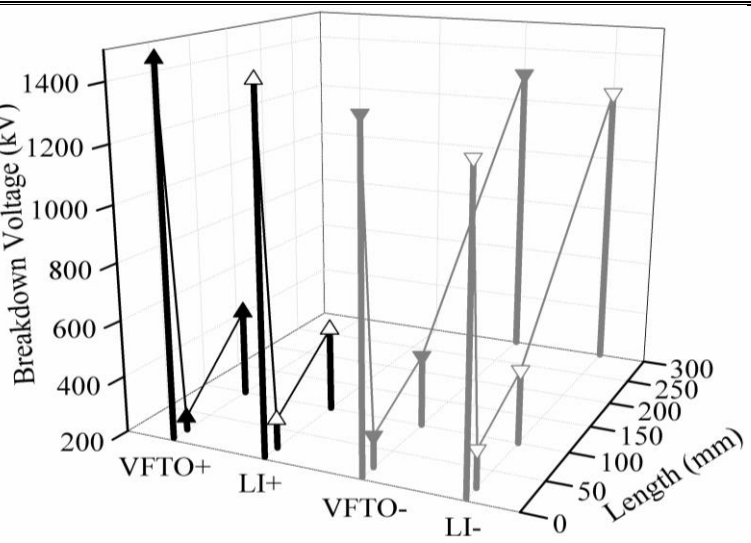

Figure 3-3. Breakdown voltage of insulaor with and without defects (p=0.5 MPa)

(a) insulator without defect under VFTO

(b) insulator with defect under VFTO (x=29 mm)

(c) insulator with defect under VFTO (x=108 mm)

(d) insulator without defect under standard LI

Figure 3-4. Discharge images of insulators with and without defects

In the paper, charge will generate with a relatively high density on insulator surface near to the needle under VFTO and LI [41]. These surface charges interact with the charges of streamer head in developing breakdown channel shown in Figure 3-5. Thus, two forces are acting on streamer head, i.e. F_t formed by the external field and F_n from the surface charges [40]. When the positive impulse was applied on inner electrode shown in Figure 3-5(a), positive charges would accumulate on insulator

surface near to the needle [41]. Thus, the streamer head near to inner electrode was attracted to the insulator surface. The interaction of the partial arc and insulator would cause damage to the insulator and a dark trace was left on insulator surface [42]. The streamer head near to outer electrode was instead pushed away from the insulator surface and insulator damage was less probably. Only the light trace was observed. These are proven by discharge traces shown in Figure 3-4(b) and Figure 3-4(c). The case that inner electrode biased negatively is shown in Figure 3-5(b). Charges could hardly accumulate on insulator surface without defect [41] and only F_t was acted on streamer head. Moreover, the field of insulator surface was more uniform because of shielding effect of the inner protruding electrode. So, the discharge could hardly develop on insulator surface near to inner electrode shown in Figure 3-4(a).

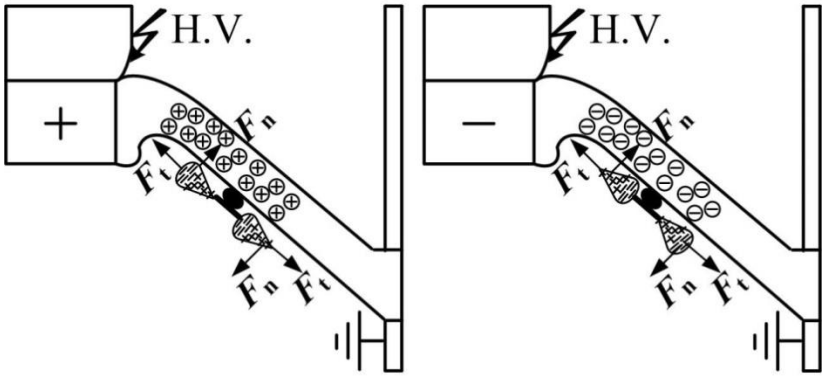

(a) positive polarity (b) negative polarity

Figure 3-5. Schematic discharge diagram of insulators with defect

In order to obtain the distribution of surface electric field of the insulator and further understand the accumulation of the surface charges, Ansoft Maxwell was used to simulate the total surface electric field $\boldsymbol{E}$, its normal component $\boldsymbol{E}_\mathbf{n}$ and tangential component $\boldsymbol{E}_\boldsymbol{\tau}$ of the insulator with and without defect, as shown in Figure 3-6. When computing, 1000 kV static voltage was stressed on the high voltage electrode. As shown in Figure 3-6(a), the distribution of surface electric field of the insulator without defect is approximately uniform. The maximal $\boldsymbol{E}$ and $\boldsymbol{E}_\mathbf{n}$ both appear on the concave side of the insulator close to the inner conductor. When the insulator is contaminated by the needle, the surface electric field increases significantly to a maximum of 6 times more than that of the insulator without defect.

Figure 3-6(b) and Figure 3-6(c) indicate that $\boldsymbol{E}_\mathbf{n}$ near the needle is much stronger than $\boldsymbol{E}_\boldsymbol{\tau}$. Large quantities of charges are accumulating in the insulator surface close to the needle, resulting where the breakdown voltage of insulator with defect decreases significantly when compared with that without defect. Apart from that, when comparing Figure 3-4(b) with Figure 3-4(c), the maximal $\boldsymbol{E}$ (x=28 mm) and $\boldsymbol{E}_\mathbf{n}$ (x=28 mm) are larger than the maximal $\boldsymbol{E}$ (x=108 mm) and $\boldsymbol{E}_\mathbf{n}$ (x=108 mm), which causes that the breakdown voltage of the needle near the high electrode is the lowest, as verified in Figure 3-3.

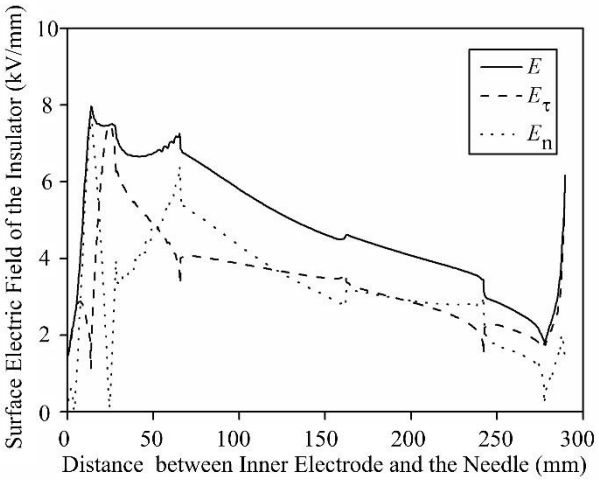

(a) Without defect

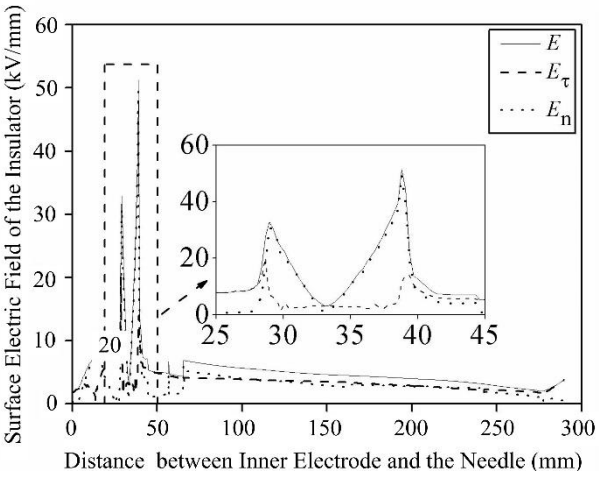

(b) With defect, x=29 mm, 1000 kV

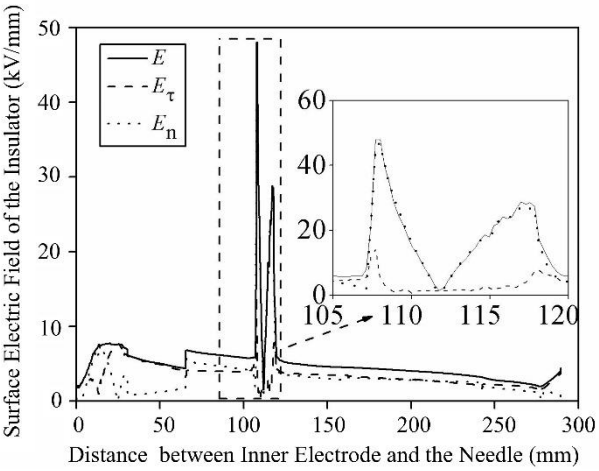

(c) With defect, x=108 mm, 1000 kV

Figure 3-6. $\boldsymbol{E}$, $\boldsymbol{E_\tau}$ and $\boldsymbol{E_n}$ of insulator

To investigate the effect of the length of the needle contaminant l on the insulator under VFTO and standard LI, various lengths of needles were used keeping the defect location x at 108 mm. Figure 3-7 shows the corresponding results of positive and

negative VFTO and LI flashover tests indicating that the 50% breakdown voltage decreases with increasing needle length. For l<15 mm, the 50% breakdown voltage under VFTO is higher than that with standard LI. However, VFTO decreases significantly for l>15 mm, compared with standard LI.

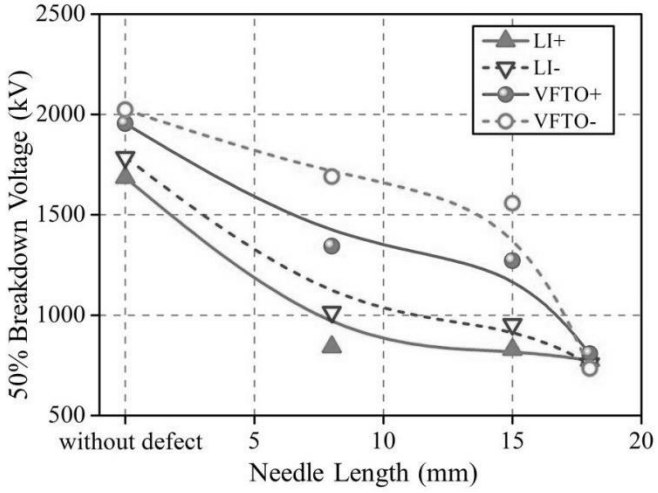

Figure 3-7. Breakdown voltage vs. needle length for insulator with defect under VFTO and standard LI(p=0.5 MPa, x=108 mm)

3.1.3 Effect of Voltage Waveform

Waveform conversion factor ***K*** was proposed [37] to clarify the effect of voltage waveform on discharge characteristics, which was defined by the ratio of 50% breakdown voltage under VFTO to that under standard LI. The factor ***K*** of rod-plane gap and insulator are shown in Figure 3-8 and Figure 3-9. It can be seen from Figure 3-8 that ***K*** for negative polarity decreases with increasing pressure and ***K*** decreases below 1 when pressure reached up to 0.5 MPa.

Previous research shows that micro discharge in the gas near insulator surface such as streamer corona caused by fixed metal particles is the prerequisite condition for charge accumulation under impulse voltage [41]. In the case of VFTO, a large number of charges are deposited onto the defective insulator surface by streamer and displacement current at the rising slope of oscillating impulse [19]. A strong reverse electrical field is formed when the impulse decreases rapidly, resulting the so called “back discharge” [43] occurs between the channel and surrounding deposited charges. Back discharge decreases the shielding effect of surface charges and also increases the conductivity of streamer channels, so that the leader can be triggered easily. Besides, the displacement current induced by oscillating impulse will generate a magnetic field parallel to the insulator surface, which will cause electrons emitted from the surface of defective insulator to be deflected toward the surface [44]. These electrons strike the insulator surface and produce secondary electron avalanche, which also strike the surface to promote the surface flashover. As a result, the breakdown voltage of defective insulator under VFTO can be lower than that under standard LI by 8% shown in Figure 3-9.

It is interesting to observe that multi-channels are formed on insulator surface when

VFTO is applied as shown in Figure 3-4(b) and Figure 3-4(c), while the discharge channels on insulator surface under LI are fewer than these under VFTO shown in Figure 3-4(d), which can be explained by the inter-shielding effect of electron avalanches. Because of the difference in the delay times of primary electrons, some preceding avalanches grow ahead and form the space charge field to distort the applied electric field, which lead to the suppression of adjacent electron avalanche called posterior avalanche. With decreasing front time of pulse, the difference in formation of primary electrons decreases, the inter-shielding effect of electron avalanches also decreases, resulting in the increase of discharge channel. Therefore, it can be clarified that the decrease of pulse front time will increase the discharge channel number.

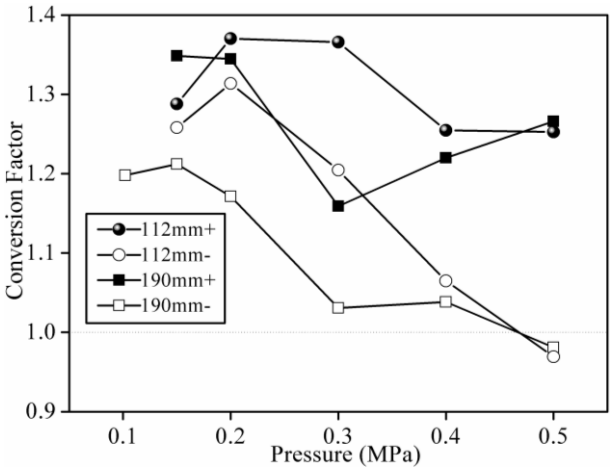

Figure 3-8. Waveform conversion factor vs. gas pressure for rod-plane gap

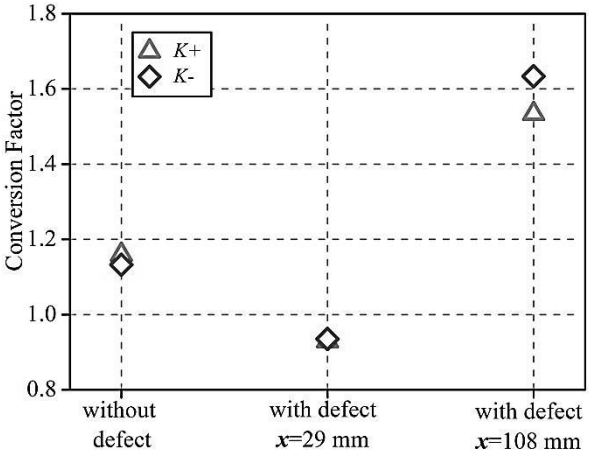

Figure 3-9. Waveform conversion factor of insulaor with and without defects

3.2 Breakdown Characteristics of Sound Insulation System

A series of investigations [45-47] have been conducted on discharge characteristics and mechanisms of SF_6 gas in GIS. But the research results of the insulation characteristics of GIS under VFTO have big dispersion and poor comparability for the

waveform parameters of VFTO have not been standardized. The actual VFTO originates from multiple times breakdown process has many parameters, such as front time, oscillation frequency, oscillating coefficient and damping coefficient [48]. Control variate method should be used to clarify the main influential parameters of VFTO on the breakdown in SF_6. In this part, based on the established impulse generating system, the discharge characteristics of SF_6 gas gaps under VFTO with different front times, wavetail damping time simulated by double-exponential impulses and different oscillating coefficients were studied.

3.2.1 Breakdown Voltage of Sound Insulation System

As is well-known that quasi-uniform electric field is used in the design of GIS to improve the electrical strength for the reason that SF_6 is sensitive to electric field. The field nonuniformity factor f is in the range of 1.67 ~ 2.22 for a sound insulation system. Figure 3-10 shows the 50% breakdown voltage vs. gas pressure of r/d = 15/15 mm rod-plane gas gap (f = 1.70) under LI with different wavefront times and wavetail times.

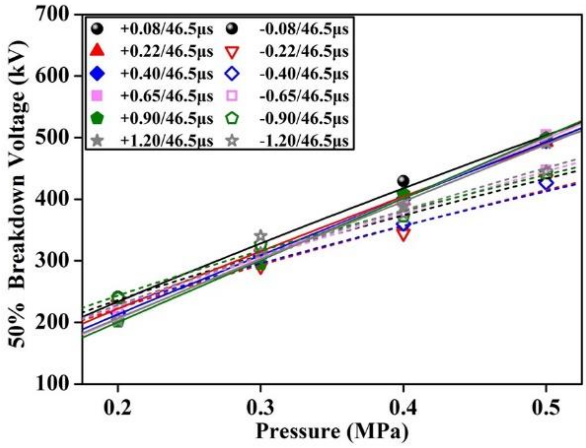

(a) different wavefront times

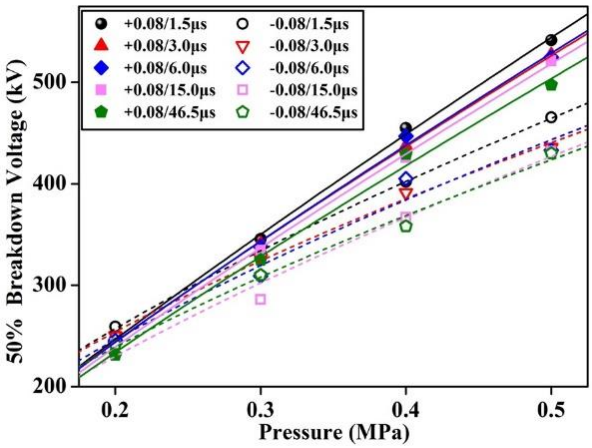

(b) different wavetail times

Figure 3-10. Breakdown voltage vs. gas pressure for r/d = 15/15 mm rod-plane gap

Those points are experimental results. Based on the experimental data, the 50%

breakdown voltages of the r/d = 15/15 mm gap were fitted by various formulas and the best one was derived as [49]

$$U_{50\%}=k(pd)^{n}/f^{m} \tag{3-1}$$

where,

$U_{50\%}$ ——the 50% breakdown voltage，kV；

k, n, m ——constants related to voltage types；

p ——gas pressure，MPa；

d ——gap distance，mm；

f ——field nonuniformity factor.

It can be seen that the 50% breakdown voltage under different impulses increases linearly with the increase of gas pressure, reflecting the property of a quasi-uniform electric field, and has an obvious polarity effect. The increasing trend of non-standard LI is similar to that of a standard LI.

When the field nonuniformity factor f increases, for example of the r/d = 15/33 mm rod-plane gap with f = 2.72, similar characteristics also appear, as shown in Figure 3-10 and Figure 3-11, using the fitting formula (3-1).

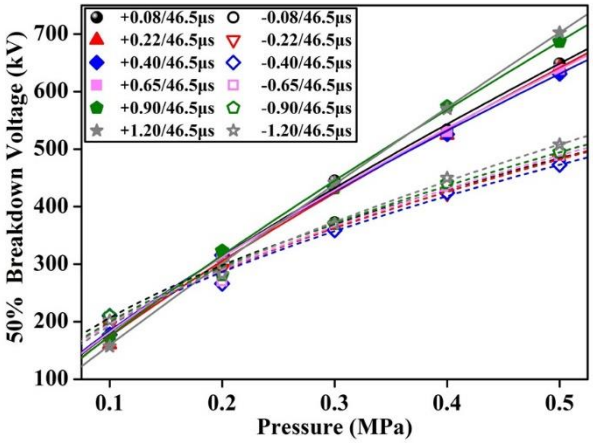

(a) different wavefront time

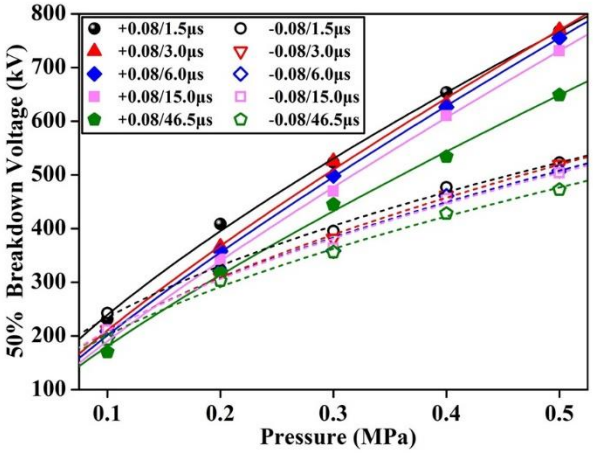

(b) different wavetail time

Figure 3-11. Breakdown voltage vs. gas pressure for r/d = 15/33 mm mm rod-plane gap.

It is worth mentioning that with the field nonuniformity factor *f* increases, the polarity effect becomes more obvious. As shown in Figure 3-11, the difference that values of 50% breakdown voltage of positive and negative polarity impulses becomes larger compared with that in Figure 3-10. The values of empirical constants obtained from *f* = 1.70 is not suitable for *f* = 2.72. The values of empirical constants of *f* = 2.72 has big difference from that of *f* = 1.70.

It is interesting to find that, from Figure 3-10 and Figure 3-11, when the pressure is lower, the breakdown voltages under negative impulses are higher than that under positive impulses, but when the pressure exceeds a certain value, the breakdown voltages under positive impulses turn out to be higher than that under negative impulses.

3.2.2 Influence of Wavefrom Parameters

Figure 3-12 shows the 50% breakdown voltage vs. waveform parameter of *r*/*d* = 15/15 mm rod-plane gas gap under LI with different wavefront times and wavetail times.

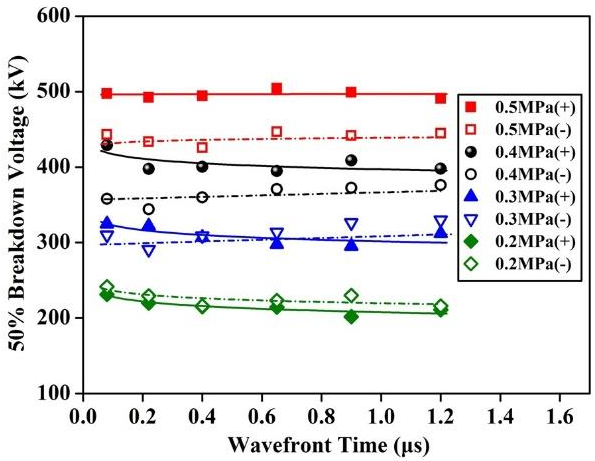

(a) in relationship with wavefront time

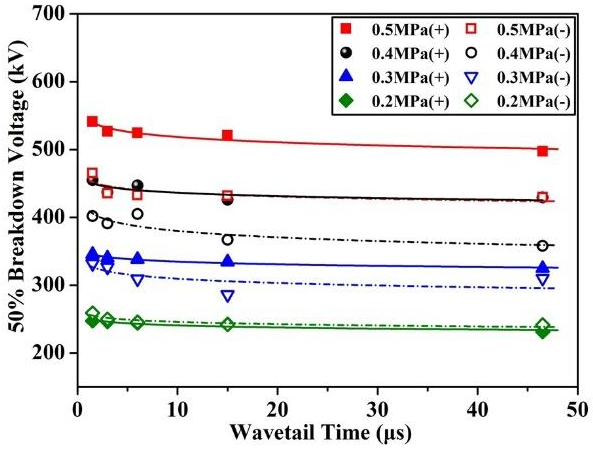

(b) in relationship with wavetail time

Figure 3-12. Breakdown voltage vs. waveform parameters for *r/d* = 15/15 mm rod-plane gap

It is not hard to find that with wavefront time increasing, the 50% breakdown

voltages have slight change. With the wavetail time increasing, the 50% breakdown voltages decrease fastly before 6 μs and gradually become flat. In other words, the LI waveforms of wavefront time less than 1.2 μs or wavetail time in the range of 6 ~ 50 μs have little influence on the 50% breakdown voltages. The LI waveform parameters have little influence on the breakdown characteristics of a sound GIS system.

Figure 3-13 shows the V-t curve of *r/d* = 15/15 mm rod-plane gap at different wavefront time impulse voltages at 0.5 MPa. It can be seen that the *V-t* curve is relatively flat after 1 μs, and the difference between the impulse voltages with different wavefront times is small. This explains from another aspect that for a quasi-uniform electric field, the impulse voltage wavefront time has little effect on its discharge characteristics.

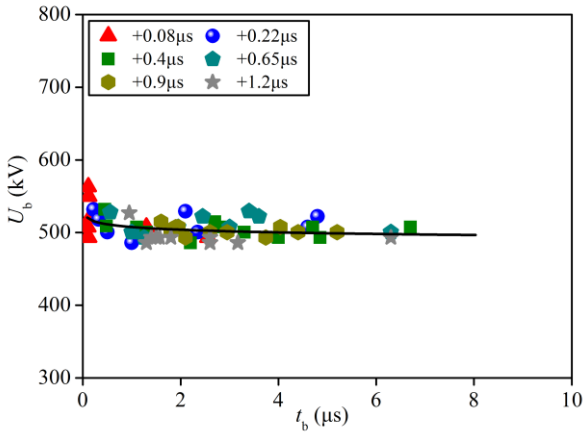

(a) positive polarity

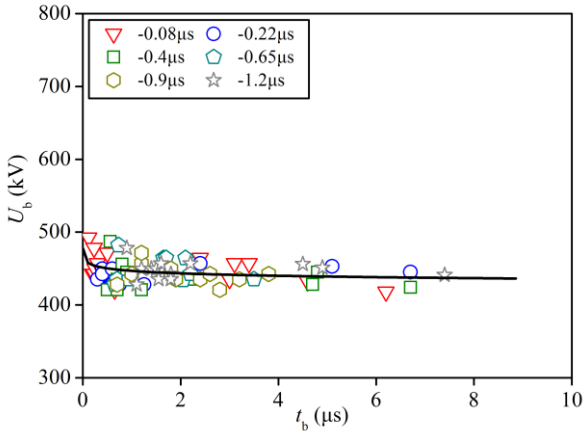

(b) negative polarity

Figure 3-13. *V-t* curves of *r/d* = 15/15 mm rod-plane gap (*p* = 0.5 MPa)

When the field nonuniformity factor *f* increases to 2.72, the waveform parameters of LI have influence on the 50% breakdown voltage with the field nonuniformity factor *f* increasing, but they are still not significant, as shown in Figure 3-14.

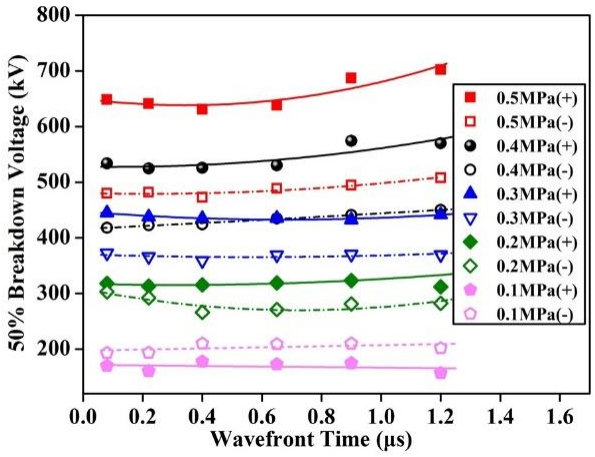

(a) in relationship with wavefront time

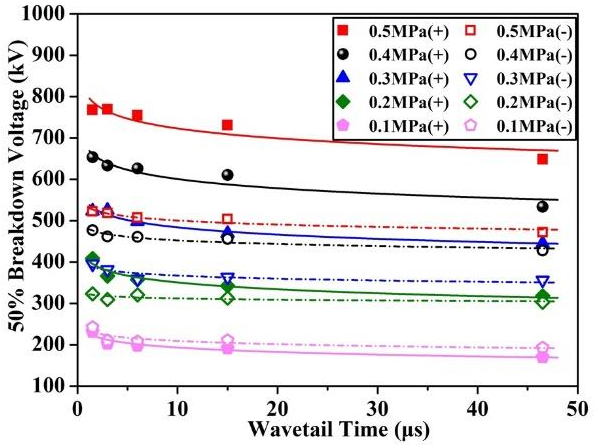

(b) in relationship with wavetail time

Figure 3-14. Breakdown voltage vs. waveform parameters for *r/d* = 15/33 mm rod-plane gap

3.2.3 Effect of Ocillating Coefficients

Figure 3-15 shows the breakdown voltage of 72 mm sphere-plane gas gap under VFTOs of different oscillation coefficients.

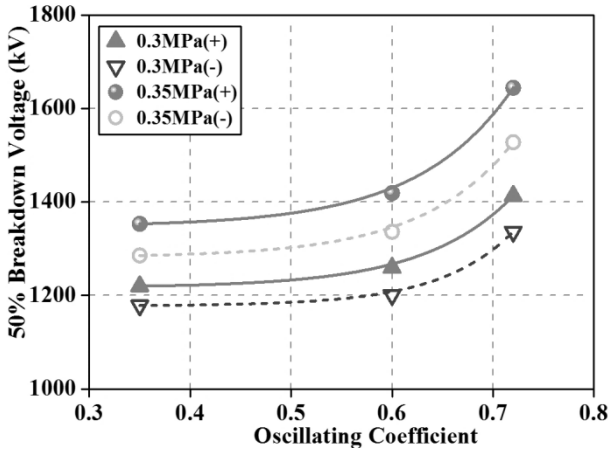

Figure 3-15. 50% Breakdown voltage vs. ξ for 72 mm sphere-plane gap under VFTOs

It can be see that the breakdown voltage increases with the increasing of ξ and the breakdown voltages in positive polarity are higher than that in negative polarity. The equal-area criterion can be used to explain the results [50, 51], as shown in equation (3-2) and Figure 3-16. Where, V_0 is the static breakdown voltage, t_0 is the instant at which $V(t)=V_0$, t_f is the period from t_0 to breakdown, and A_f is a constant that depends on the gap conditions and other factors. For the same peak value waveforms and similar breakdown delay time, the lower the is, the larger the effective area is.

$$\int_{t_0}^{t_0+t_f} \{V(t)-V_0\}\,dt = A_f\,[\mathrm{V\cdot s}] \tag{3-2}$$

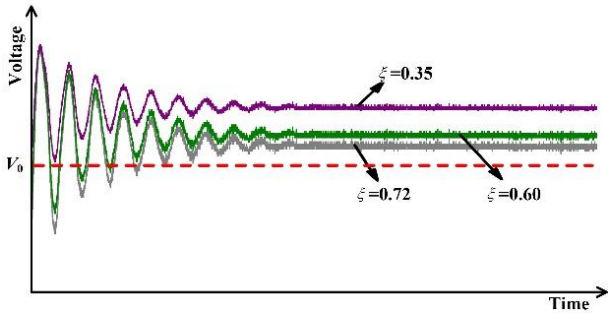

Figure 3-16. Concept of equal-area criterion for VFTO

3.3 Breakdown Characteristics of System With Defects

For a GIS well designed, it does not fail unless a defect of some sort is present, which implies an inhomogeneous electric field appears in the system. Impulse test is also used for detecting these insulation defects.

3.3.1 Breakdown Voltage of System With Defects

The r/d = 2/33 mm rod-plane gap with f = 12.17 was used to simulated the local electric field enhancement defects possibly caused by a metallic conducting particle attached in the bus. Figure 3-17 shows 50% breakdown voltages under LI with different wavefront times and wavetail times at different gas pressures. The increasing trend is significantly different from that of a quasi-uniform electric field, not the linear trend. With a rise of gas pressure, the hump phenomenon occurs in the $U_{50\%}$ - P curves, and the polarity effect is very obvious, as shown in Figure 3-17(b). The 50% flashover voltage of the post insulator with a metal particle defect at different pressures was also investigated. Figure 3-18 shows the variation of the positive and negative 50% flashover voltages of the post insulator under different double-exponential impulses. The hump phenomenon also appears.

3.3.2 Influence of Wavefrom Parameters

Figure 3-19 shows the 50% breakdown voltage vs. wavefront time of r/d = 2/33 mm rod-plane gas gap. It is not hard to find that with the wavefront time increasing,

the 50% breakdown voltages have remarkable change and the $U_{50\%}$ - T_f curve tends to be U-shaped. To have a better understanding of the U-shaped curve, the statistical time lag, the corona formation time, the leader stepping time and the corona stabilization need to be considered. The T_f corresponding to the lowest 50% breakdown voltage can be defined as the critical wavefront time T_c. It needs a time lag to make the gap broken down. When $T_f < T_c$, the discharge time lag t_d decreases with the decrease of T_f. The effective area of the impulse decreases with the decrease of t_d for the same voltage amplitude value. Therefore, it needs to increase the voltage amplitude value to reach the effective area which is constant for a certain electrode and gas pressure [50, 51]. So the 50% breakdown voltage increases with the decrease of T_f. When $T_f > T_c$, effect of the impulse steepness on the t_d decreases. However, with the increase of T_f, the corona stabilization effect is strengthened, which will increase the breakdown voltage. So the 50% breakdown voltage increases with the increase of T_f. The critical wavefront time T_c is in the range of 0.2 to 0.7 μs. Compared with r/d = 15/15 mm, it can found that the larger the electric field factor f is, the more obvious the U-shaped trend is. In order to further prove this conclusion, another two electrodes with higher field nonuniformity factor f were tested, as shown in Figure 3-20.

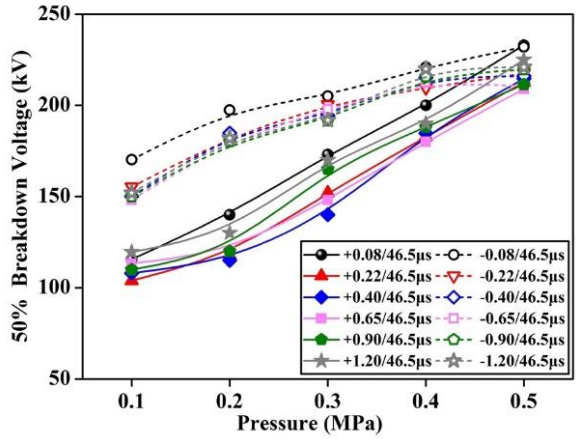

(a) different wavefront time

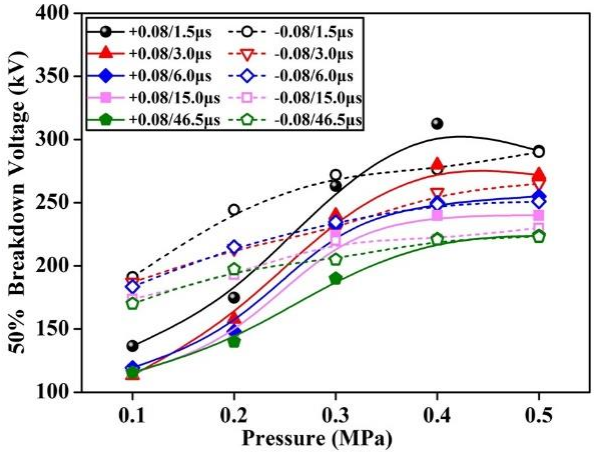

(b) different wavetail time

Figure 3-17. Breakdown voltage vs. gas pressure for r/d = 2/33 mm mm rod-plane gap

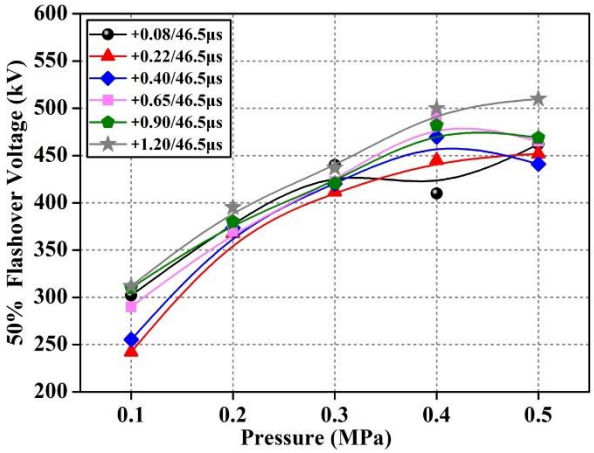

(a) positive polarity

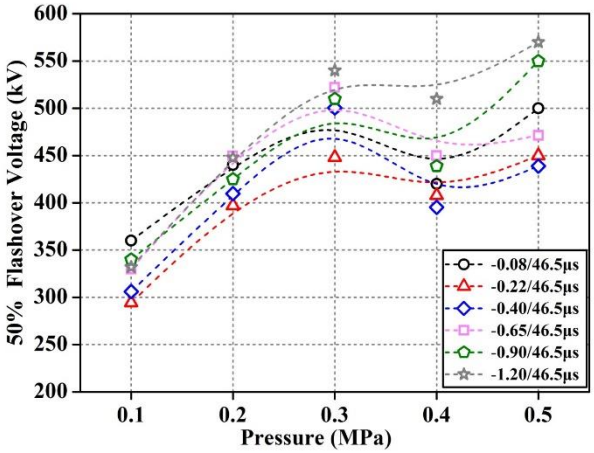

(b) negative polarity

Figure 3-18. 50% flashover voltage vs. gas pressure for insulators with defects

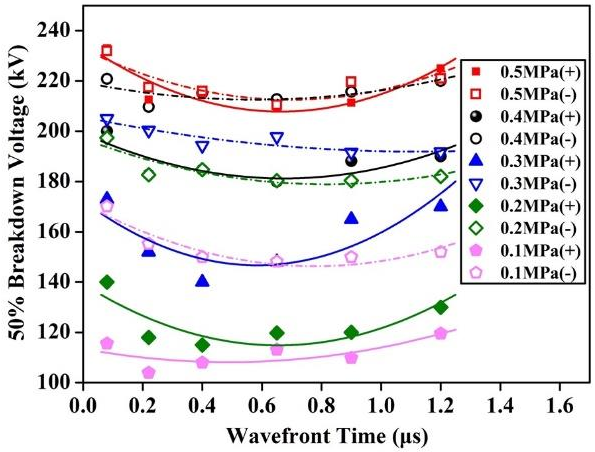

Figure 3-19. Breakdown voltage vs. wavefront time for r/d = 2/33 mm rod-plane gap

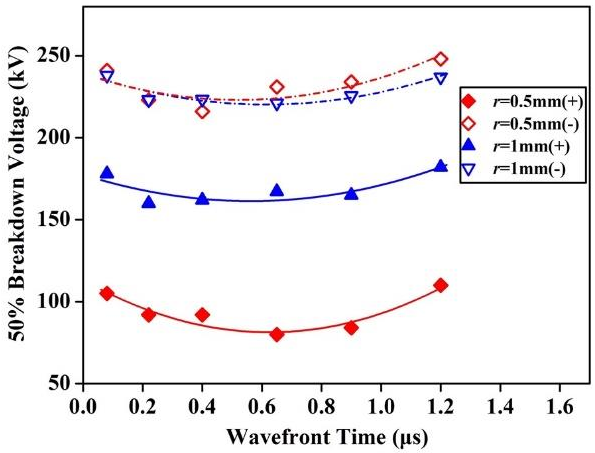

Figure 3-20. Breakdown voltage vs. wavefront times for *r/d* = 1/33 mm and *r/d* = 0.5/33 mm rod-plane gaps at 0.5 MPa

Figure 3-21 shows the *V-t* curves of *r/d* = 2/33 mm rod-plate under impulse voltage with different wavefront times at 0.5 MPa pressure. Compared with Figure 3-13, along with the decrease of breakdown delay time, the *V-t* curve rises up more obviously. The result shows that the breakdown voltage of highly inhomogeneous electric field gap is very sensitive to discharge time delay. However, the discharge delay time is greatly affected by the wavefront time.

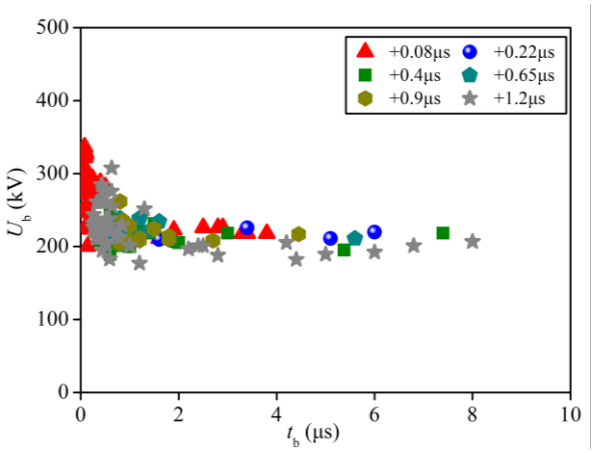

(a) positive polarity

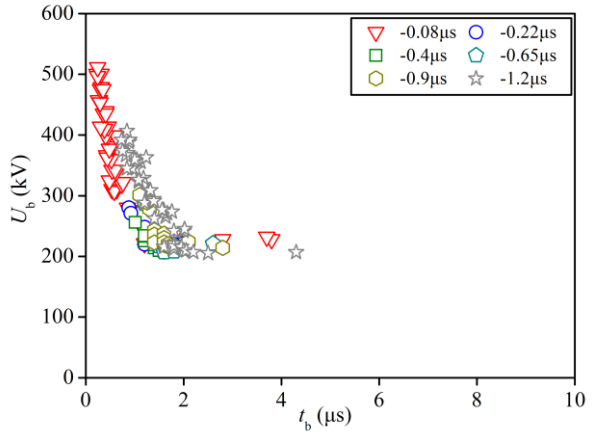

(b) negative polarity

Figure 3-21. *V-t* curves of *r/d* = 2/33 mm rod-plane gap (*p* = 0.5 MPa)

The effect of impulse wavefront time on the surface flashover voltage of post insulator with a metal particle attached on the surface was studied, as shown in Figure3-22. It can be seen from Figure 3-22 that the breakdown voltage vs. wavefront time curves also show a U-shaped trend generally.

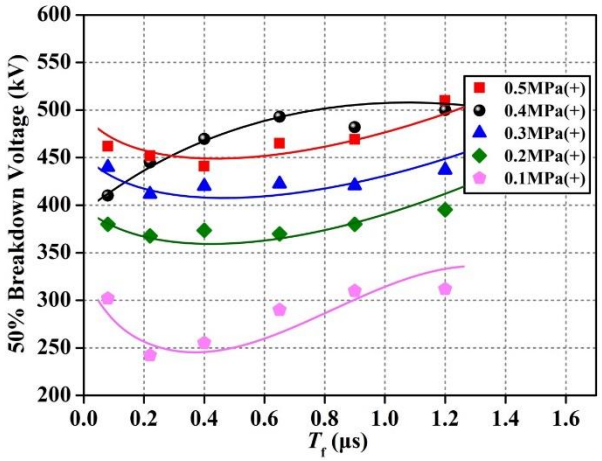

(a) positive polarity

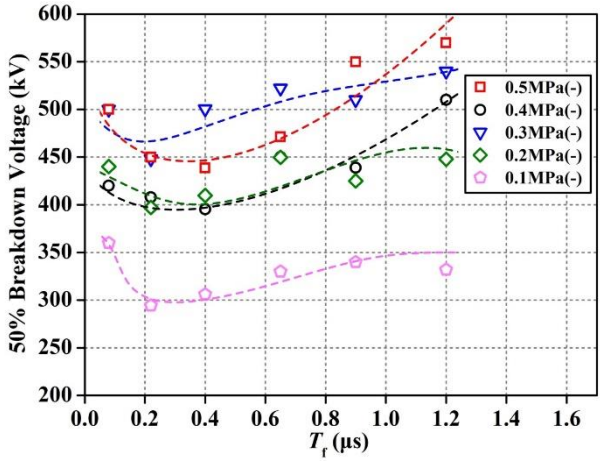

(b) negative polarity

Figure 3-22. 50% flashover voltage vs. wave front time for insulators

Figure 3-23 and Figure 3-24 show the 50% breakdown voltage vs. wavetail times of r/d = 2/33 mm rod-plane gas gaps. The 50% breakdown voltages decrease significantly with the increase of impulse wavetail time, especially when the wavetail time is in the range of 1.5 to 15 μs, but the difference of the values decreases after 15 μs, which could also be explained by the area method. Assuming that the discharge time lag is t_d, the static discharge voltage is U_0 (the corresponding time is t_0), the effective areas for these five impulses can be calculated by equation (3-3), where A_f is a constant depending on the gap conditions and other factors. For the same impulse voltage U(t), the difference values of the adjacent two impulses are A_{21}, A_{32}, A_{43} and A_{54}, as shown in Figure 3-25. It can be easily found that $A_{21} > A_{32} > A_{43} > A_{54}$. So with the wavetail time increasing, the discharge voltage difference reduces.

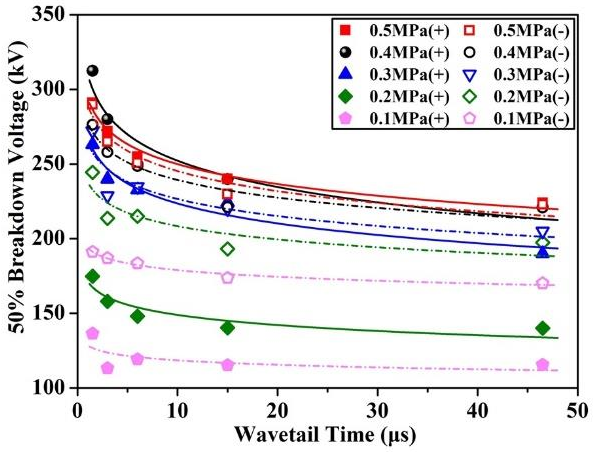

Figure 3-23. Breakdown voltage vs. wavetail time for *r/d* = 2/33 mm rod-plane gap

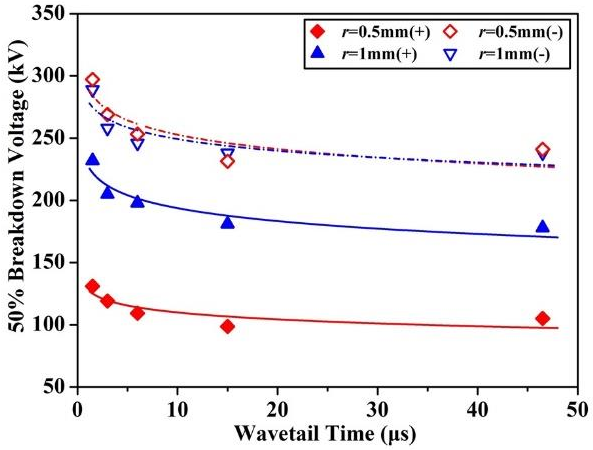

Figure 3-24. Breakdown voltage vs. wavetail times for *r/d* = 1/33 mm and *r/d* = 0.5/33 mm rod-plane gaps at 0.5 MPa

$$\int_{t_0}^{t_d} \{U(t) - U_0\}\, dt = A_f \tag{3-3}$$

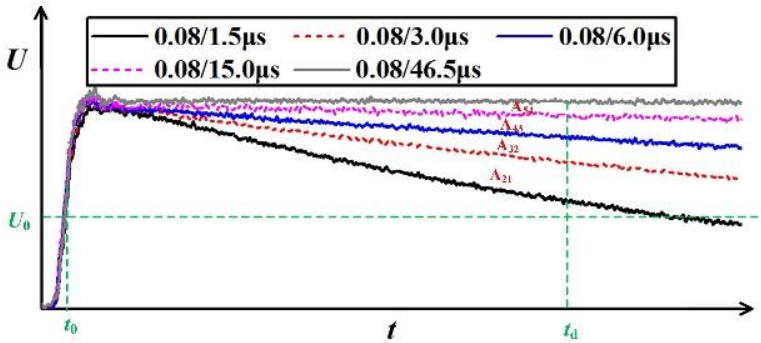

Figure 3-25. 50% breakdown voltages decrease with the increase of impulse wavetails explained

3.4 Effect of Voltage Polarity

For a quasi-uniform electric field, especially the rod-plane gap with $1 < f < 2$, breakdown voltage is usually observed higher when the rod electrode is stressed by

positive polarity voltages, which is opposite for a non-uniform electric field. However, the polarity effect for the rod-plane gap in this thesis has been found to be different, as shown in Figure 3-1, Figure 3-10， Figure 3-11 and Figure 3-17. When the pressure is lower, the breakdown voltages under negative impulses are higher than that under positive impulses, but when the pressure exceeds a certain value, the breakdown voltages under positive impulses turn out to be higher than that under negative impulses for all electrodes both with quasi-uniform electric field and highly inhomogeneous electric field. This interesting phenomenon called "polarity reversion" can be explained by diagram shown in Figure 3-26.

An electron avalanche, as shown in stage 1 of Figure 3-26, will be created if the electric field is sufficiently high. The electrons and positive ions contained in the avalanche will drift in opposite directions under the applied field $E_0(x, t)$. The heavier positive ions will move slowly toward the cathode. The electrons, as shown in stage 2 of Figure 3-26, will disappear in anode when positive polarity voltage is applied. They will form negative ions when the applied voltage of rod electrode is negative polarity. Once the streamer is triggered, a large number of ions will accumulate in streamer channels and the electric field distributions $E_2(x, t)$ at higher pressures are shown in stage 3 of Figure 3-26. For positive polarity, $E_2(0, t) < E_0(0, t)$, so the avalanche is hard to be created. While for negative polarity, $E_2(0, t) > E_0(0, t)$. The electronegative gas of SF_6 is easy to form the negative ion-cluster, which is hard to drift and diffuse due to its big mass and volume. Thus, the negative ion-clusters accumulate in front of the streamer channel, causing severe field distortion. The new avalanche is created easily and $E_2(0, t)$ as well as $E_2(x_2, t)$ increases continually with the increase of space charges injection, resulting ease in propagating of streamer further into the gap. Thus, the breakdown voltage of SF_6 in negative polarity is lower than that in positive polarity. The polarity effect is related to the gas pressure and field nonuniformity factor *f*. The critical pressure of polarity reversion may be related to electric field inhomogeneity: it increases with the increase of electric field inhomogeneity, proved by Figure 3-17(a), the 50% breakdown voltage of positive polarity will be higher than that of negative polarity when the gas pressure exceeds 0.5 MPa, larger than that for quasi-uniform electric field around 0.15 MPa from Figure 3-1. The phenomenon can be explained as follows. With the decrease of the electrode's curvature radius *r* (the rise of *f*), the corona inception voltage is lower at the same gas pressure, resulting in a more quantity of electric charge injected by streamer corona. After migrating and proliferating, the uniform effect of space charge for the electric field is stronger. So a high gas pressure is needed to restrain the corona stabilization effect.

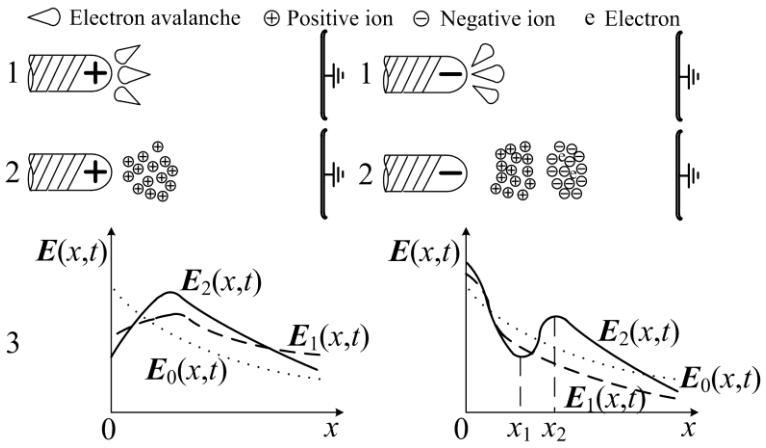

(a) Positive polarity (b) Negative polarity

1-formation of electron avalanches 2-redistribution of space charges

3-electtric field distributions

Figure 3-26. Schematic diagram of polarity effect

3.5 The Critical Radius Phenomena

Figure 3-27 shows the breakdown voltage in relationship with electrode curve radius for 33 mm rod-plane gaps under LI with different wavefront times and wavetail times at 0.5 MPa. It is found that the discharge characteristics of SF_6 gas gap present a so-called critical radius effect which occurs in long gap discharge in air [52, 53]. With the decrease of electrode radius, the breakdown voltage of the gap decreases till a so-called critical radius is reached, and then remains practically constant for further reduction of curve radius.

The critical radius effect is obvious for negative polarity. The critical radius is around 2 mm or more from the limited experimental data. But the critical radius effect does not occur for the positive polarity and the critical radius may be less than 0.5 mm. The influence of voltage polarity on the critical radius can be explained by the size of streamer corona and the migration and diffusion of space charges under different voltage polarities. On one hand, the streamer initial voltages under negative polarity are lower than those under positive polarity, but the breakdown voltages under negative polarity are close or high than those under negative polarity at 0.5 MPa based on the experimental data. So the streamer can be developed more sufficiently, causing a lager streamer corona size. On the other hand, the electron is easier to migrate and diffuse under negative polarity, hence negative space charge could be formed in a greater scope. Therefore, the critical radius, related to the streamer corona size, has a bigger value under negative polarity than that under positive polarity.

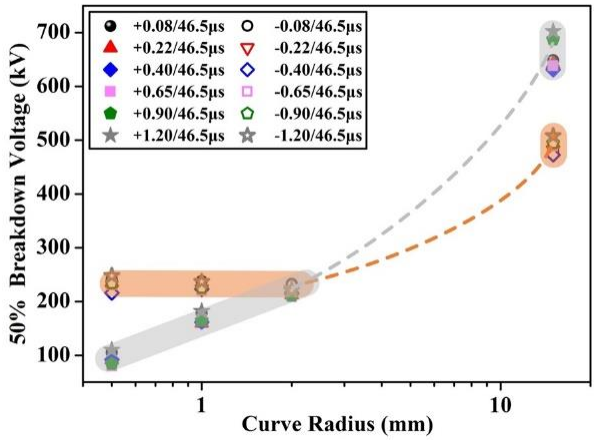

(a) under LI with different wavefront times

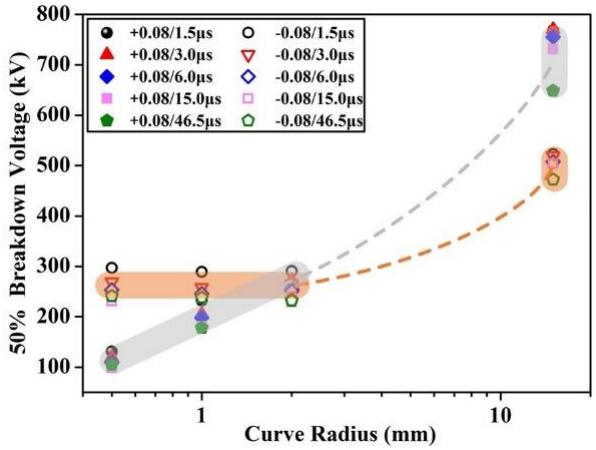

(b) under LI with different wavetail times

Figure 3-27. Breakdown voltage vs. electrode curve radius for 33 mm rod-plane gaps at 0.5 MPa

3.6 Brief Summary

1) The breakdown voltage for VFTO or standard LI in positive polarity is higher than that in negative polarity and the breakdown voltage of VFTO could be lower than that of standard LI at high gas pressure. The breakdown voltage of insulator under VFTO or standard LI in negative polarity is higher than that in positive polarity and the breakdown voltage of defective insulator under VFTO could be lower than that under LI by 8%.

2) The LI waveform parameters have significant influence on the breakdown characteristics of GIS system with defects. The $U_{50\%}$ - T_f curve tends to be U-shaped.

3) The 50% breakdown voltage vs. gas pressure shows the polarity reversion phenomenon, which can be explained by the migration and diffusion of space charges. The critical pressure of polarity reversion may increase with the increase of electric field inhomogeneity.

4) The discharge characteristics of SF_6 short gas gap has a critical radius phenomenon similar as long air gap. The critical radius under negative polarity is bigger than that under positive polarity.

CHAPTER 4. DISCHARGE CHARACTERISTICS OF SF_6 GAS UNDER IMPULSE VOLTAGES WITH WIDE RANGE WAVEFRONT TIME

LI waveform is widely used in the impulse test. According to the breakdown characteristics of SF_6 in a highly inhomogeneous electric field, it can be concluded that the LI waveform parameters have significant influence on the breakdown characteristics of GIS system with defects. Compared with the influence of wavetail time, wavefront time should be paid more attention for the difficult in generating a wanted impulse in the field due to large inductance and test load capacitance. In this chapter, considering the real LI test waveform, the discharge characteristics of SF_6 gas under impulse votlages with wide range wavefront time were studied.

4.1 The Necessity of On-site Lightning Impulse Test

Two kinds of main insulation defect types in GIS equipment may occur in the process of transportation and installation: one is the unfixed insulation defects formed by internal freedom conductive particles and dust; the other is the fixed insulation defects formed in the transportation and installation process [54]. Therefore, the on-site withstand voltage and insulation detection test, as the final pass before the GIS equipment been put into operation, is very important to improve the quality of the power grid.

In recent years, AC withstand voltage and partial discharge test has become the main means of insulation detection to ensure the reliable operation of power equipment. But for electric equipment, especially the GIS equipment, AC withstand voltage and partial discharge test is not effective to find all the defects, which is one of the main reasons for the frequent insulation breakdowns of GIS in recent years. For example, Qinghai 330 kV Antong switching station, which had passed the AC withstand voltage test, had insulator flashover accident while being put into operation. After collapsed, it is found that the internal cleanliness of the tank is not enough and a lot of dust adhered on the insulator surface. In addition, similar to Antong switching station, basin-type insulator surface flashover accident occurred in Li Jiaxia hydropower station 363 kV GIS, which has been put into operation in quite a long time. In the hand-over test of the three gorges hydropower station 550 kV GIS, the equipment passed the AC withstand voltage test. But three flashover accidents occurred during the impulse test process. The facts above show that AC withstand test and partial discharge test have some limitations in detecting the defects of local field concentration in GIS.

For high voltage SF_6 gas, breakdown phenomenon in highly uniform electric field

is abnormal. The AC or DC breakdown voltage increases with pressure up to a maximum value firstly. Then they fell to a minimum and continue to rise again. In the range of the project operation pressure, the relationship of breakdown voltages of SF_6 highly inhomogeneous electric field and gas pressure presents an abnormal phenomena called “hump” phenomena[55], as shown in Figure 4-1.

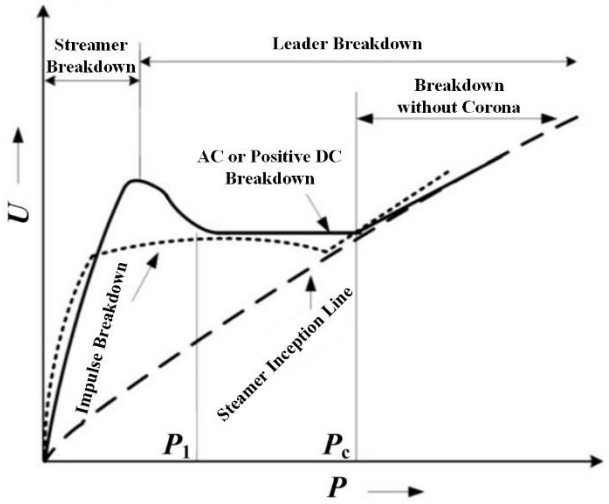

Figure 4-1. Typical *U*-*P* curve for SF_6 highly inhomogeneous electric field

When $P < P_c$, corona discharge happens before gap breakdown. And partial discharge detection system can detect the discharge signal. But when $P > P_c$, there is no corona discharge before gap breakdown. The breakdown voltage and corona inception voltage are similar. Once corona discharge happened, the gap is breakdown immediately. However, the working gas pressure of GIS in the power system is higher than Pc. So the partial discharge rarely appears before the insulation breakdown. This is why the AC partial discharge test is very difficult to find the GIS insulation defects. Therefore, it is necessary to add new examination methods, complemented with AC withstand voltage and partial discharge test, to provide comprehensive final detection before the GIS equipment been put into operation.

On-site LI test of GIS equipment is also recommended in IEC 62271-203 and GB 7674-2008 for 245 kV and above [27, 57]. One of the following two test procedures shall be chosen:

Procedure B (recommended for 245 kV and above): Power-frequency voltage test for a duration of 1 min at the specified test voltage; partial discharge measurements at specified power-frequency test voltage.

Procedure C (recommended for 245 kV and above, alternative to procedure B): Power-frequency voltage test for a duration of 1 min at the specified test voltage; LI tests with three impulses of each polarity and with the specified voltage value.

Although IEC and GB recommend on-stie LI tests for GIS equipment of 252 kV and above, there are few reports on on-site LI tests for GIS, especially for UHV GIS equipment. Usually, the on-stie oscillating LI withstand voltage test is carried out in China as shown in Table 4-1. And the typical test waveforms are shown in Figure 4-2.

Table 4-1. On-site oscillating LI test case for GIS

Time	Voltage class	Test value	Wavefront time
2007	550 kV	1240 kV	10 μs ~ 11.7 μs
2008	363 kV	940 kV	6.41 μs ~ 6.9 μs
2008	800 kV	1680 kV	10.98 μs ~12 μs
2008	800 kV	1680 kV	8.1 μs ~9.32 μs
2014	1100 kV	1920 kV	12.74 μs ~ 13.13 μs

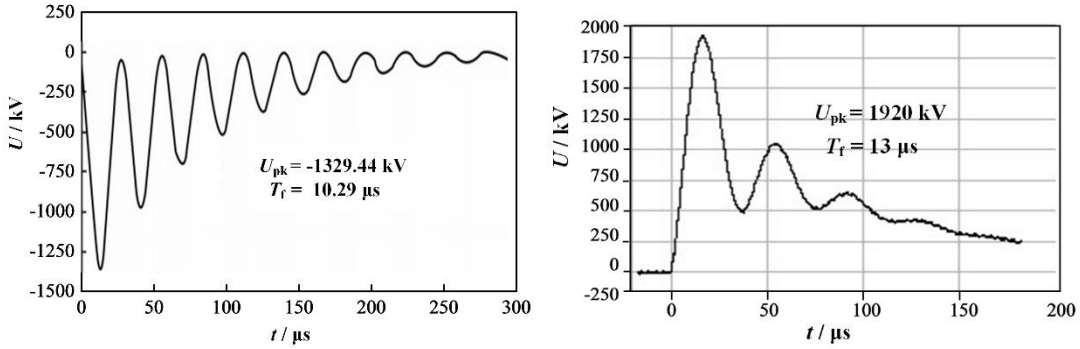

(a) 550 kV GIS, 2007 (b) 1100 kV GIS, 2014

Figure 4-2. Typical waveform of oscillating LI test

4.2 Discharge Characteristics under Oscillating LI

Usually, a non-standard LI test for GIS in the field called oscillating LI (OLI) test with long T_f is preferred for the easy obtained and high output efficiency η. The on-site oscillating LI test has been carried out in the Three Gorges hydropower station 550 kV GIS, especially in the Zhe-Fu ultra high voltage (UHV) GIS substation, in China. A typical waveform of the oscillating LI, as shown in Figure 2-4, is an impulse with a long T_f and tens of oscillating frequency.

Figure 4-3 shows relationship of 50% breakdown voltage and gas pressure under standard LI (SLI) and oscillating LI. In the range of 0.3-0.6 MPa, the 50% breakdown voltages of oscillating LI are higher than those of standard LI by 15.6%, 11.5%, 18.0% and 12.7% respectively. In other words, the local electric enhancement, like a particle defect, which can be detected by standard LI, may not be detected by oscillating LI.

The main differences between these two impulses are in the steepness of the wave and the oscillatory nature of the wave. Figure 4-4 shows the typical breakdown waveforms of SLI and OLI. Figure 4-5 shows the breakdown voltage as a function of time-to-breakdown under these two impulses. It is not hard to find that the breakdowns for oscillating LI almost occur in the front of the waveform, which is different for the standard LI with short T_f. Figure 4-6 shows relationship of 50% breakdown voltage and gas pressure under impulse with T_f = 10 μs and oscillating LI. The two impulses have a similar T_f and 50% breakdown voltage. Therefore, it can be inferred that the T_f plays an important role in the insulation defect detecting

effectiveness. The following research is focused on the effect of T_f.

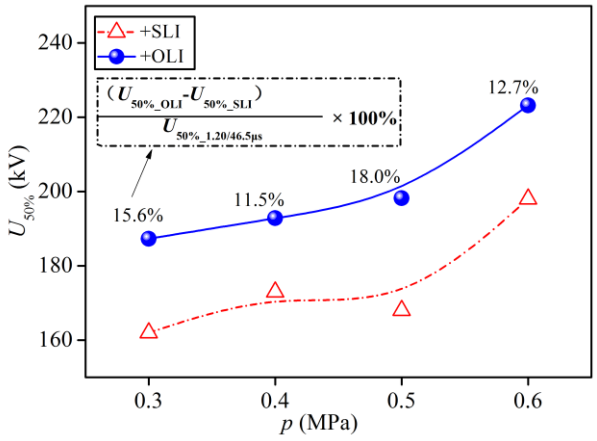

Figure 4-3. 50% breakdown voltage vs. gas pressure under standard LI and oscillating LI for 60 mm rod-plane gap

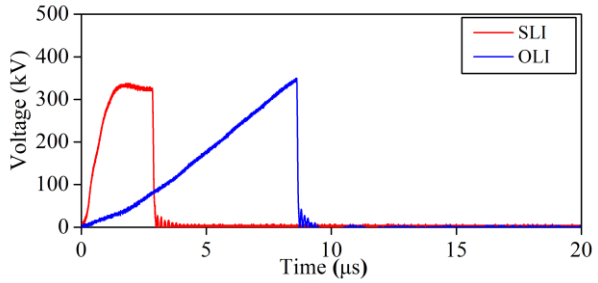

Figure 4-4 Typical breakdown waveforms of SLI and OLI.

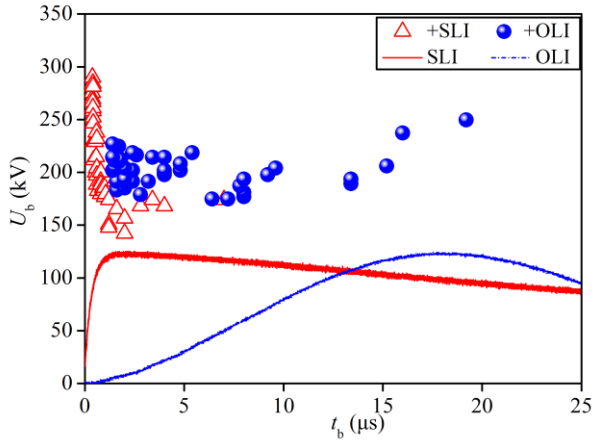

Figure 4-5. Breakdown voltage as a function of time-to-breakdown under standard LI and oscillating LI at an SF_6 pressure of 0.6 MPa for 60 mm rod-plane gap

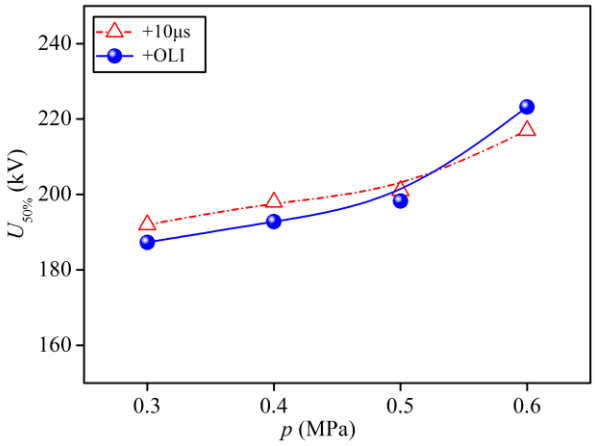

Figure 4-6. 50% breakdown voltage vs. gas pressure under impulse with T_f = 10 μs and oscillating LI for 60 mm rod-plane gap

4.3 Effect of Wavefront Time in a Wide Range

Figure 4-7 shows the 50% breakdown voltage vs. double-exponential impulse wavefront times T_f in the range of 0.08 ~ 23.5 μs at 0.6 MPa for rod-plane gaps with different gap distance. It can be seen that with T_f increases, the 50% breakdown voltages have an increased trend. Especially when T_f exceeds 2.0 μs, the 50% breakdown voltage is higher than that of standard LI obviously.

Figure 4-8 shows the breakdown voltage as a function of time-to-breakdown under four different wavefront times 0.08, 1.2, 10 and 23.5 μs at an SF_6 pressure of 0.6 MPa for 33, 45 and 60 mm rod-plane gaps. Usually, the time-to-breakdown decreases with the increase of the breakdown voltage, as the trends for T_f=0.08, 1.2 μs. However, it is interesting to see that the time-to-breakdown increases with the increase of the breakdown voltage for T_f=10, 23.5 μs, which is opposite for the short T_f=0.08, 1.2 μs. Those points are experimental results. Based on the experimental data, the V-t curve can be fitted by

$$\log U_b = a + b\log t_b + c\left(\log t_b\right)^2 \tag{4-1}$$

where, U_b is the breakdown voltage in kV. t_b is the time to breakdown in μs. a, b, c are constants related to electrode structure and gas pressure. The fitting lines are shown by solid line in Figures 4-6 Formula (4-1) is undoubtedly suitable for highly inhomogeneous field in the test range. In Formula (4-1), a represents $\log U_b$ when t_b = 1 μs; $2c$ can represent the changing rate of the curve slope. Based on Formula (4-1), only three dates (U_b, t_b) can picture the V-t curve of the gas gap. In order to obtain an accurate curve, t_b of the dates should be distributed in a large range.

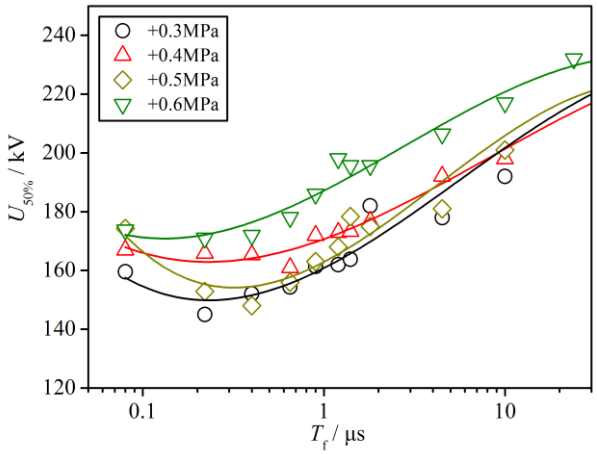

Figure 4-7. 50% breakdown voltage vs. double exponential impulse wavefront times T_f in the range of 0.08 - 23.5 μs at 0.6 MPa for rod-plane gaps

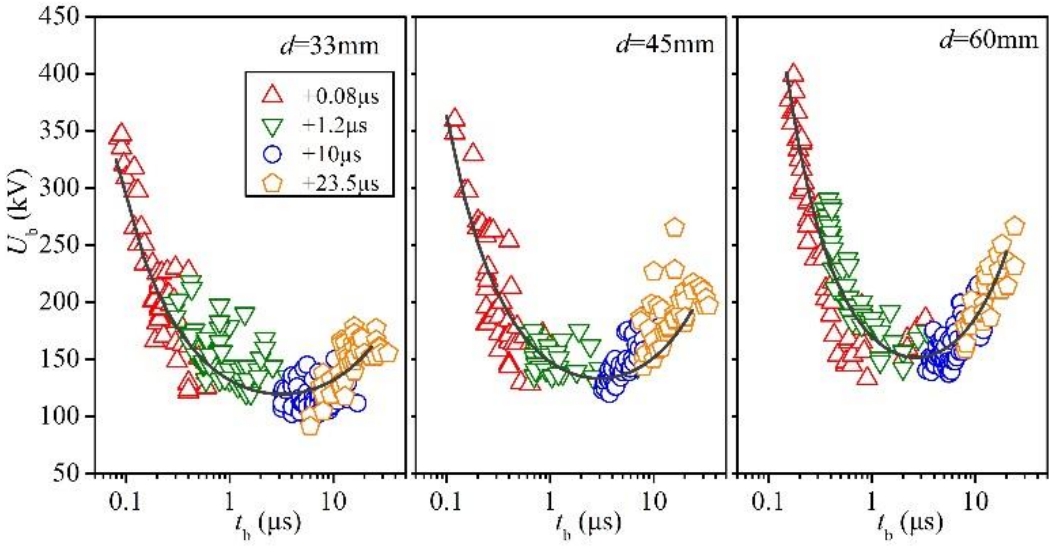

Figure 4-8. Breakdown voltage as a function of time-to-breakdown under four different wavefront times at an SF_6 pressure of 0.6 MPa for rod-plane gaps

Another interesting phenomenon can be found that for T_f = 0.08 μs, the breakdowns all happen in the tail. But the breakdowns mostly occur in the front or near the peak for impulses with long T_f, especially when T_f = 10, 23.5 μs, which makes the breakdown voltage value is lower than the prospective voltage value. In order to further study the insulation defect detecting effectiveness, the Y-axis "Breakdown Voltage" of Figure 4-8 should be changed to "Prospective Voltage", as shown in Figure 4-9. The prospective voltage can be calculated by equation (2-2) for the breakdowns occur in the front. From Figure 4-9, it can be seen clearly that the minimum breakdown voltages U_{BDmin} increases with the increase of T_f (except for d = 33 mm), which can directly indicate that the insulation defects detecting effectiveness decreases with the increase of T_f from the point of the minimum breakdown voltages U_{BDmin}.

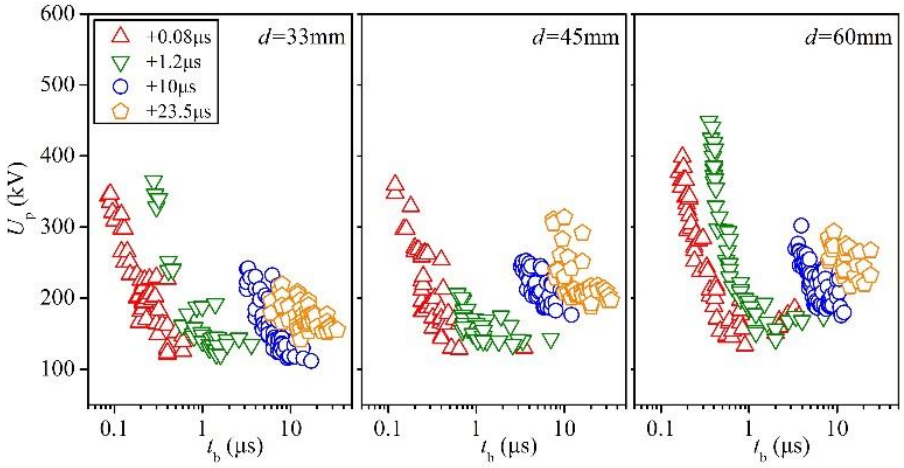

Figure 4-9. Prospective voltage as a function of time-to-breakdown under four different wavefront times at an SF_6 pressure of 0.6 MPa for rod-plane gaps

4.4 Discharge Characteristics of SF_6 Gas with Insulator

Basin-type insulators are used as insulating supports for coaxial busbar structures in GIS. Their electrical insulation performance is of crucial importance for the stability and safety of GIS switchgear. The research team also used a 126 kV basin-type insulator with a coaxial cylindrical electrode structure to investigate whether the SF_6 surface discharge under impulses with different wave front times has the same rule as the gas gap discharge. Figure 4-10 shows 50% flashover voltage vs. double exponential impulse wavefront times for basin-type insulator insulator with defect. From Figure 4-10, it can be seen that the 50% flashover voltage of the insulator with surface conductive defects increases with the increase of wavefront time, which is similiar with the results of gas gap.

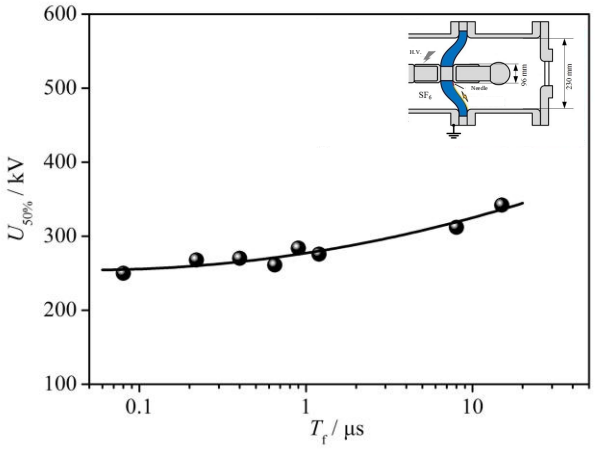

Figure 4-10. 50% flashover voltage vs. double exponential impulse wavefront times T_f in the range of 0.08 - 23.5 μs at 0.6 MPa for basin-tye insulator

4.5 Effect of Rise Rate of Impulse

For impulse with long T_f, the breakdowns almost occur in the front. The effect of T_f is the effect of the slope of impulse dU/dt essentially. The breakdown voltage U_b can

has a relationship with the slope of impulse dU/dt, as shown in Figure 4-11. With the dU/dt increase, the U_b decreases. On one hand, for SF_6 highly inhomogeneous electric field, the discharge follows streamer/leader model. The displacement current flows through the streamer channel, which is induced by steep wavefront, injecting charges into streamer tip. The charges build up at the streamer tip will enhance the electric field, which will promote the transformation of streamer to leader. For increasing impulse steepness, breakdown voltage will decrease from the viewpoint of the streamer to leader transition[57]. On the other hand, it can be explained by the effect of corona stabilization. Corona stabilization in SF_6 results in a delay of the discharge development and furthermore in an enhancement of the streamer inception and breakdown voltage. For impulse with low dU/dt, the changing rate of electric field E is low, under which the space charge can have an enough time to migration and diffusion before breakdown. The fully migration and diffusion of space charge can strengthen the shielding effect, and then increases the breakdown voltage. This can also explain the right rising part of the V-t curve. Meanwhile, for a settled (U_b, t_b), the prospective voltage value U_p can be calculated by Formula (2-2). Therefore, the longer the T_f, the higher the U_p. This trend can be found in Figure 4-11 for T_f = 10 and 23.5 μs.

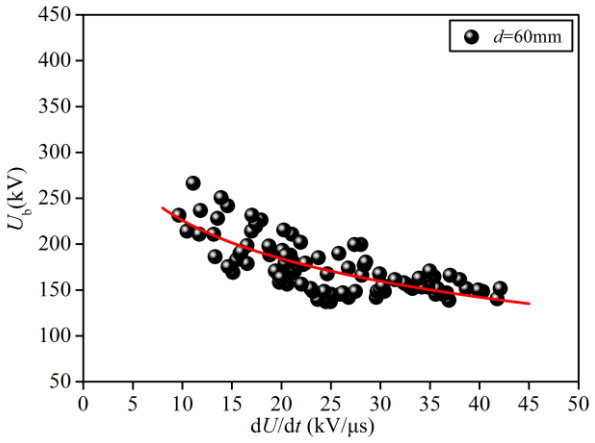

Figure 4-11. U_b vs. dU/dt at 0.6 MPa for 60 mm rod-plane gaps under T_f = 10, 23.5 μs

At streamer or discharge inception, the area A in Figure 4-12 exceeds the critical value [58, 59]. Then the critical volume V_{cr} becomes ionized, conducting and charged so that the internal field is reduced to almost E_{cr}, and the remaining ionization balances the drain of ions and electrons due to their field drift. Corona stabilization is caused by space charge formation ahead of the critical volume V_{cr}. Hence, the criterion for corona stabilization is simplified by the following condition [60].

$$v_I \geq v_{cr.m} \tag{4-2}$$

Where, v_I is the ion velocity at the boundary of the critical volume, $v_{cr.m}$ is the maximum value of the growth velocity at the beginning.

$$v_{\mathrm{I}} = \frac{b_{\mathrm{I}}}{p}\left(\frac{E}{p}\right)_{\mathrm{cr}} p = b_{\mathrm{I}}\left(\frac{E}{p}\right)_{\mathrm{cr}} = 620 \text{ m/s} \tag{4-3}$$

$$v_{\mathrm{cr.m}} = \dot{x}_{\mathrm{cr}} = \frac{1}{2}\frac{\dot{E}_{\mathrm{m}}}{E_{\mathrm{cr}}} r_t \tag{4-4}$$

Where b_{I} is the field and pressure independent ion mobility. $\dot{E}_{\mathrm{m}}$ is the changing rate of $E_{\mathrm{m}}(t)$. Assuming the impulse as a beveled wave voltage, $E_{\mathrm{m}}(t)$ can be written as $E_{\mathrm{m}}(t) = \dot{E}_{\mathrm{m}} \cdot t$. Put the Formula (4-3) and (4-4) into the Formula (4-2), then the final criterion for corona stabilization is obtained:

$$\dot{E}_{\mathrm{m}} r \frac{1}{p} = \frac{\mathrm{d}U}{\mathrm{d}t} \cdot \frac{fr}{dp} \le 109.65 \ \frac{\mathrm{kV}}{\mathrm{MPa} \cdot \mu\mathrm{s}} \tag{4-5}$$

From Formula (4-5), it can be seen that the corona stabilization is not just in relationship with the rise rate of impulse, but also with electrode structure and gas pressure. For impulse with steep wavefront, the discharge process under certain conditions also exist corona stabilization. The phenomenon of “hump phenomenon” in the discharge of SF_6 gas in a highly inhomogeneous electric field is related to the distribution characteristic of space charge in the discharge process, and it can also reflect the corona stabilization effect in some degree.

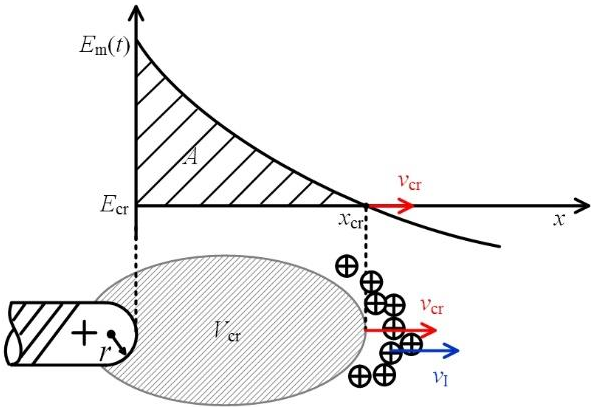

Figure 4-12. Streamer and field distribution at the tip of a rod.

Figure 4-13 shows relationship of 50% breakdown voltage and gas pressure of needle-plate electrodes under impulses with T_{f} = 0.08 μs and 15 μs. When T_{f} = 15 μs, L = 10 mm, the $U_{50\%}$-p curve has a significant hump phenomenon, indicating that there is an obvious corona stabilization. When decreasing T_{f} to 0.08 μs (T_{f} = 0.08 μs, L = 10 mm), the $U_{50\%}$-p curve does not show a hump phenomenon, as well as corona stabilization. However, when decreasing the length of the needle to L = 3 mm (T_{f} = 0.08 μs, L = 3 mm), which will also decrease the field nonuniformity factor f for the shielding effect of the GIS bus, the $U_{50\%}$-p curve shows a hump phenomenon, reflecting a certain corona stabilization effect. So the critical slope of impulse for corona stabilization $(\mathrm{d}U/\mathrm{d}t)_{\mathrm{cr}}$ for different gaps can be calculated, as shown in Table 4-2. Figure 4-14 shows the $\mathrm{d}U/\mathrm{d}t$ of impulses with different T_{f} for for 33, 45 and 60 mm rod-plane gaps. The picture indicates that the effect of corona stabilization occurs

when T_f = 10 and 23.5 μs, and in some cases when T_f = 1.2 μs, but not occurs when T_f = 0.08 μs.

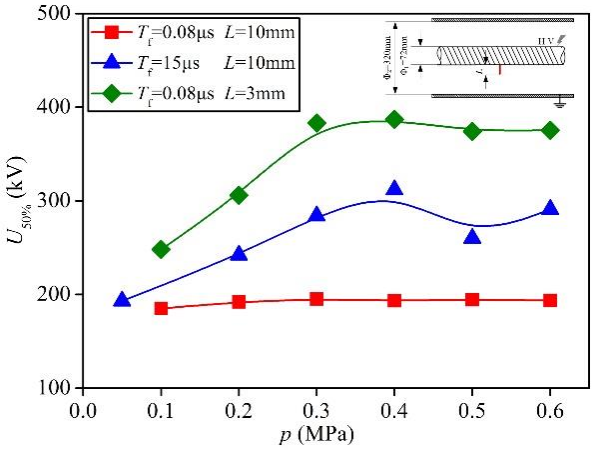

Figure 4-13. Relationship of 50% breakdown voltage and gas pressure of needle-plate electrodes under impulses with T_f = 0.08 μs and 15 μs.

Table 4-2. The critical slope of impulse for corona stabilization $(dU/dt)_{cr}$.

d/mm	p/MPa	r/mm	f	$(dU/dt)_{cr}$/kV·μs^{-1}
33			30.48	142
45	0.6	0.5	35.46	167
60			42.57	185

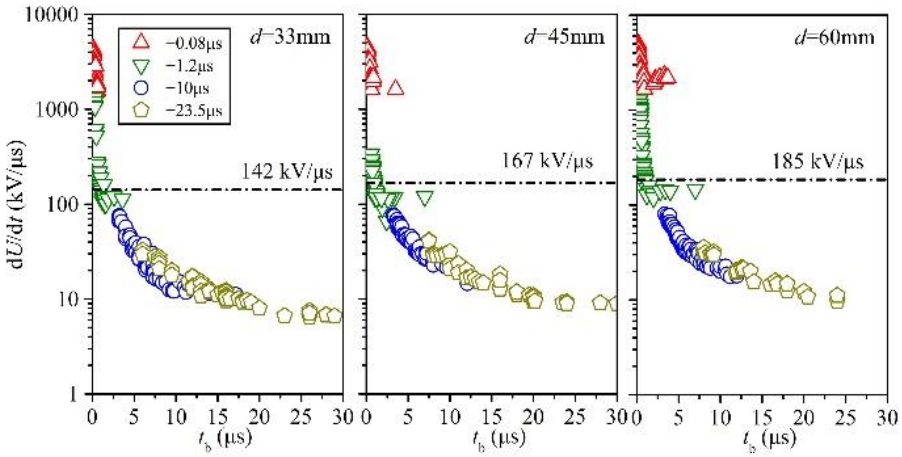

Figure 4-14. dU/dt of impulses with different T_f for for different gaps.

Figure 4-15 shows the effect of impulse slope for different gaps. For impulses with slopes of k_1 and k_2, the breakdown voltage has a difference ΔU. With the changing rate of the V-t curve increase, ΔU becomes bigger. Obviously, ΔU (d = 60 mm) $>\Delta U$ (d = 45 mm) $>$ ΔU (d = 33 mm). Here, ΔU can reflect the sensitiveness of the gap breakdown voltage for dU/dt. Therefore, for SF_6 gaps with a longer gap distance d or a higher field nonuniformity factor f, the changing rate of the V-t curve is bigger, causing a biggerΔU, which reflects that these gaps are more sensitive to dU/dt, also to T_f.

In a word, for ultra-high-voltage (UHV) GIS, which has a long gap distance, and where a defect may cause a more serious effect on electric field distribution, the changing rate of the V-t curve slope is higher. That is to say the T_f of impulse has much more influence on the defect detecting effectiveness.

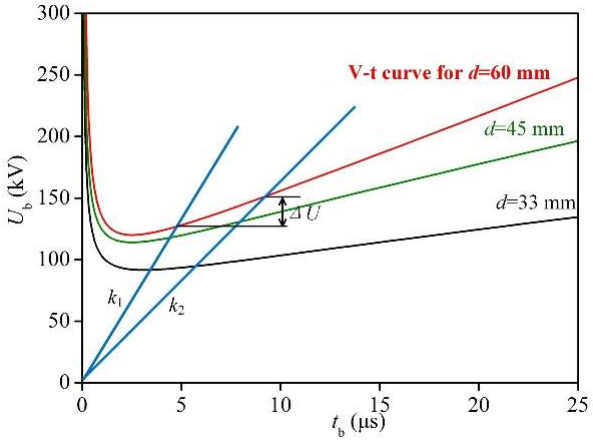

Figure 4-15. Effect of impulse slope on breakdown voltage for different gaps

4.6 Brief Summary

1) The insulation defects detecting effectiveness of oscillating LI with long Tf around 10 μs is lower than that of standard LI. According to the voltage-time characteristic, it can be inferred that the T_f plays an important role in the insulation defect detecting effectiveness. With T_f increases, the 50% breakdown voltages for rod-plane gaps have an increased trend.

2) The V-t curves of rod-plane gap under short T_f and long T_f present an opposite trend. The V-t curve shows a U-shaped in a wide range of t_b. The gap distance (or field nonuniformity factor) influences the shape of V-t curve. With the gap distance increase, the flat part of the curve and the mouth of the U-shaped V-t curve become narrower.

3) The effect of T_f is the effect of the slope of impulse dU/dt essentially. SF_6 gaps with a higher field nonuniformity factor f are more sensitive to dU/dt, also to T_f. Corona stabilization effect is not just in relationship with the rise rate of impulse, but also with electrode structure and gas pressure. The critical dU/dt for corona stabilization is calculated for different rod-plane gaps.

CHAPTER 5. EFFECT OF ELECTRODE STRUCTURE ON DISCHARGE CHARACTERISTICS

The electrode structure will influence the electric field distribution, hence influence the discharge characteristics. In this chapter, the effect of gap distance, the effect of shieding electrode has been studied. And the discharge characteristics of real defect model is researched.

5.1 Effect of Gap Distance

There is big difference in structure size of GIS for different voltage classes. The effect of gap distance should be considered in the research of detecting effectiveness. Figure 5-1 shows the standardized 50% breakdown voltage by SLI vs. double exponential impulse wavefront times T_f in the range of 0.08 - 23.5 μs at 0.6 MPa for 33, 45 and 60 mm rod-plane gap. Obviously, there is something different for the growth trend through careful comparison. It seems like that the trend for d = 60 mm grows fast than the others. The gap distance here also can reflect the field nonuniformity factor. Figure 5-2 shows the standardized 50% breakdown voltage by d = 33 mm vs. field nonuniformity factor f at 0.6 MPa for rod-plane gaps. For impulse with short T_f, with the increase of f, the $U_{50\%}/U_{50\%\_d=33mm}$ decreases faster than those impulses with long T_f.

Figure 5-3 shows the fitted V-t curves by Formula (3-3) at an SF_6 pressure of 0.6 MPa for 33, 45 and 60 mm rod-plane gaps. The values of empirical constants under different gap distances are shown in Table 5-1. From Figure 5-2, it can be seen that with the gap distance d increase, the rising part of the V-t curve is more obvious, especially for the right rising part when T_f is long. The phenomenon can also be verified from the value of 2c, which reflects the changing rate of the curve slope. And the flat part of the curve and the mouth of the U-shaped V-t curve become narrower.

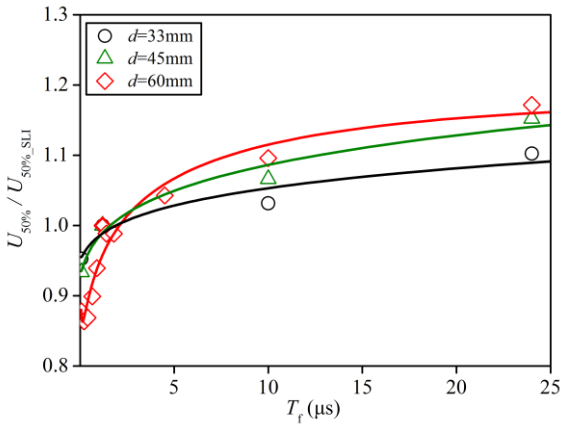

Figure 5-1. $U_{50\%}/U_{50\%\_SLI}$ vs. T_f in the range of 0.08 - 23.5 μs at 0.6 MPa for rod-plane gaps

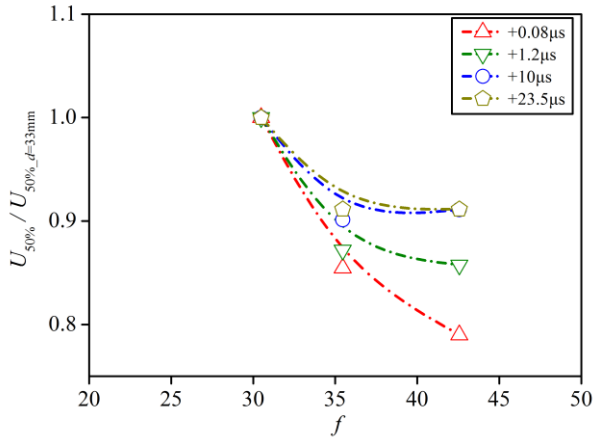

Figure 5-2. $U_{50\%}/U_{50\%\_d=33mm}$ vs. f at 0.6 MPa for rod-plane gaps

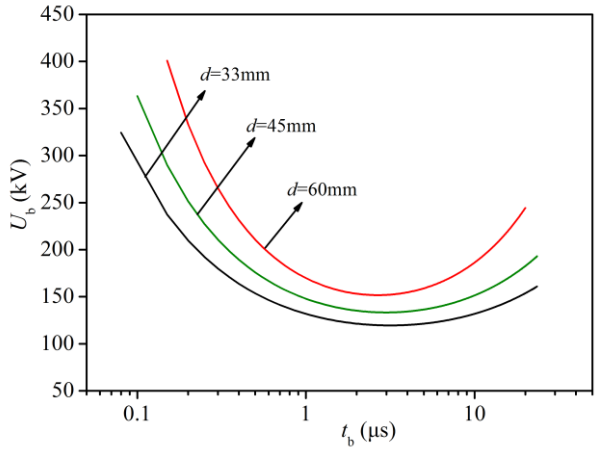

Figure 5-3. Fitted V-t curves at an SF_6 pressure of 0.6 MPa for 33, 45 and 60 mm rod-plane gaps

Table 5-1. The values of empirical constants under different gap distances

d/mm	*a*	*b*	*c*	2*c*
33	2.12	-0.17	0.17	0.34
45	2.17	-0.19	0.20	0.40
60	2.23	-0.23	0.27	0.54

5.2 Shielding Effect of Background Electric Field

In the above studies, the typical rod-plane gap was used to simulate the local electric field concentration caused by defects in GIS. The parameters of rod-plane gap is easy to be adjusted, and it is also a common form of electrode structure used by scholars at home and abroad. However, for the local electric field concentration defects in GIS, such as bus with conductive burrs attached, the gap electric field distribution is affected by background electric field. Therefore, in this section, the effect of the shielding electrode on the discharge voltage is studied by using the bus-plate electrode structure with fixed clearance distance and variable defect length.

5.2.1 Effect of Gas Pressure

Figure 5-4 shows the 50% breakdown voltage vs. gas pressure under impulses

with different T_f for coaxial cylinder structure with different needle length L.

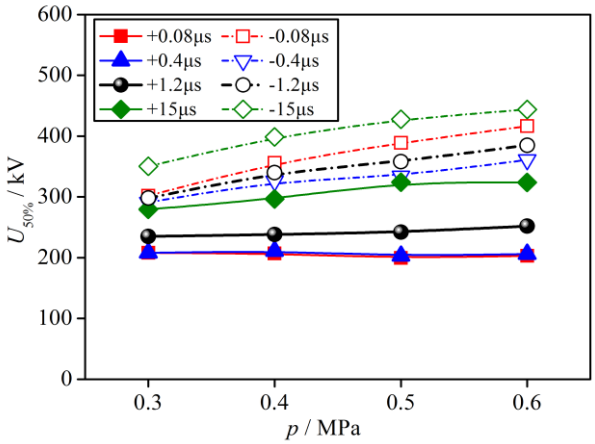

(a) L = 3 mm, D = 33 mm

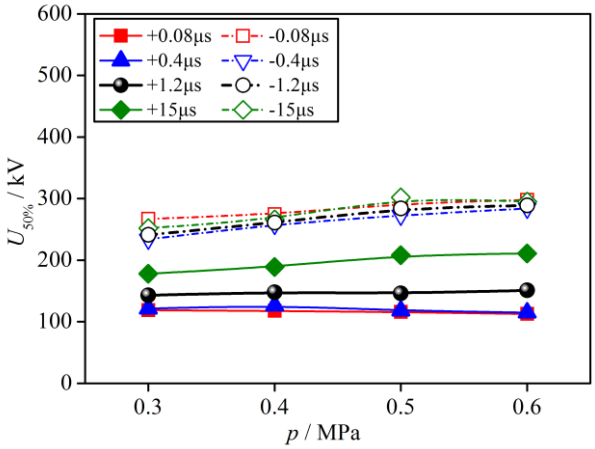

(b) L = 10 mm, D = 33 mm

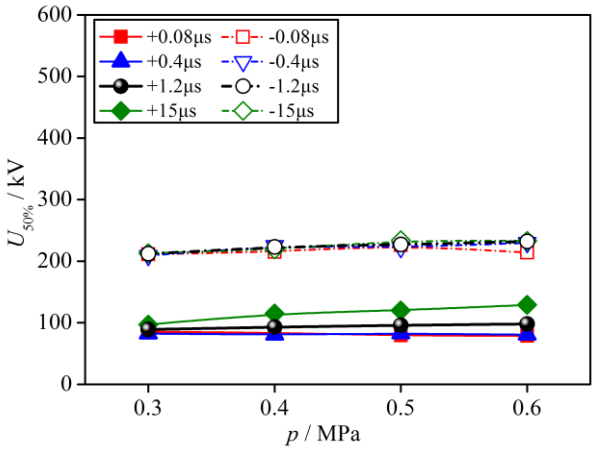

(c) L = 40 mm, D = 33 mm

Figure 5-4. 50% breakdown voltage vs. gas pressure under impulses with different T_f for different needle length L

It can be seen from Figure4-4 that the polarity effect is very significant for the needle electrode with extremely small curvature radius. Within the pressure range of 0.3 MPa to 0.6 MPa, the negative discharge voltage is higher than the positive polarity.

The reversal of polarity effects has not yet appeared. Comparing positive and negative $U_{50\%}$-p curves, it can be found that positive discharge voltage is less influenced by gas pressure. Meanwhile, the discharge voltage at T_f = 15 μs increases more significantly with the gas pressure than that at T_f = 0.08 and 0.4 μs. It can be explained that the long wavefront time enhances the effect of space charge on the electric field.

5.2.2 Effect of Needle Length

Figure 5-5 shows the 50% breakdown voltage vs. needle length L under impulses with different T_f. When the gap distance is constant, the longer the defect length, the lower the discharge voltage. This phenomenon fully shows that when the gap distance and the defect scale are consistent, the discharge voltage of the SF_6 gas gap is greatly influenced by the shielding electrode. The influence effect is basically determined by the gap electric field distribution. When L increases from 3 mm to 10 mm, the discharge voltage drops obviously. When L is further increased, the discharge voltage decreases slowly.

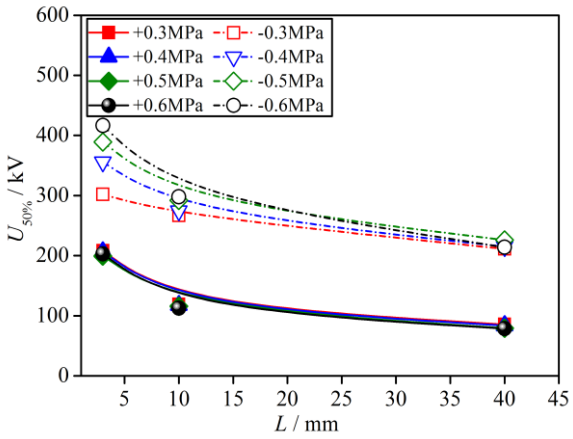

(a) T_f = 0.08 μs

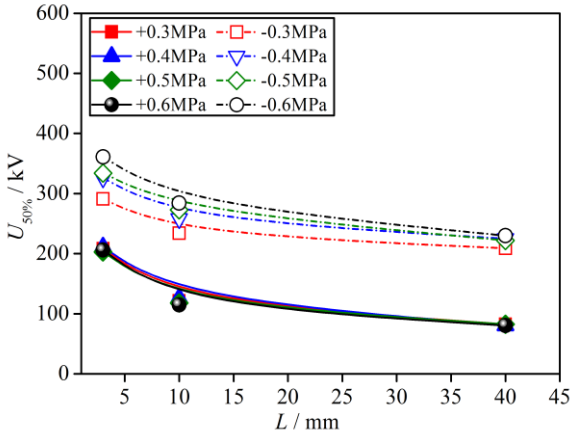

(b) T_f = 0.4 μs

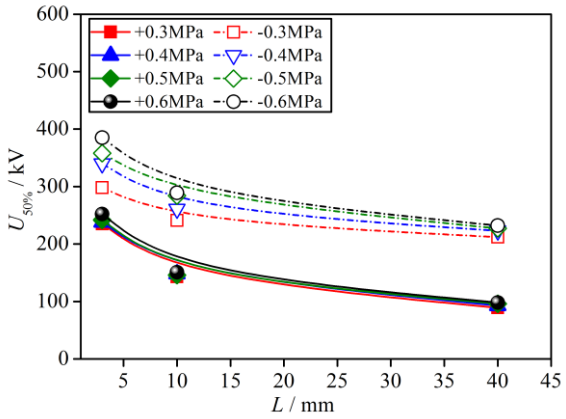

(c) T_f = 1.2 μs

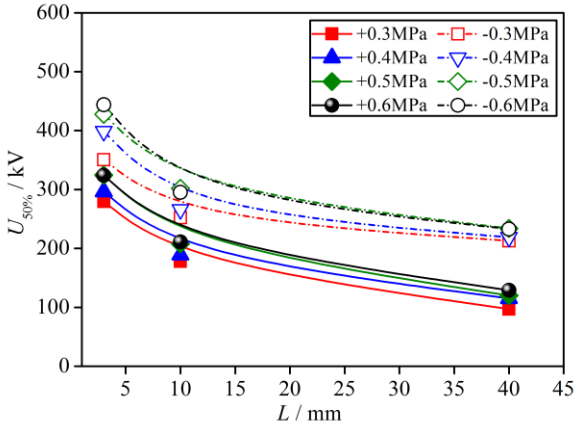

(d) T_f = 15 μs

Figure 5-5. 50% breakdown voltage vs. needle length L under impulses with different T_f

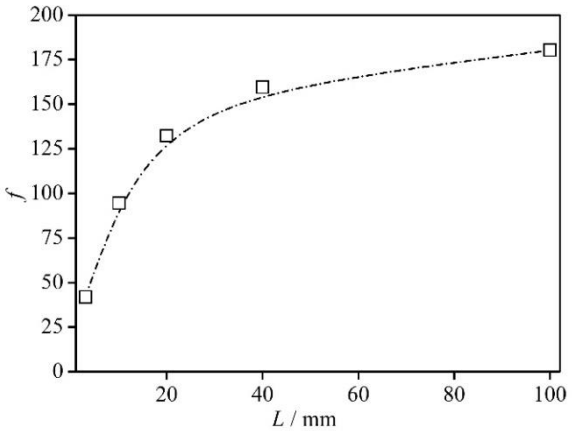

Figure 5-6. Electric field nonuniformity coefficient under different L

5.2.3 Effect of Wavefront Time

Figure 5-7 shows the 50% breakdown voltage vs. T_f for different needle length L. Compared with the negative polarity, the gap discharge voltage with positive polarity impulse voltage changes more obviously with the wavefront time increase. With the increase of wavefront time, the discharge voltage of the gap increases, which is different from U-shape of $U_{50\%}$-T_f curve for rod-plane gap as shown in Figure 4-5.

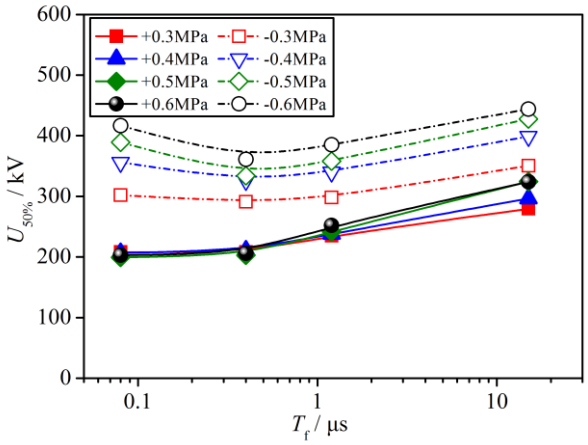

(a) L = 3 mm, D = 33 mm

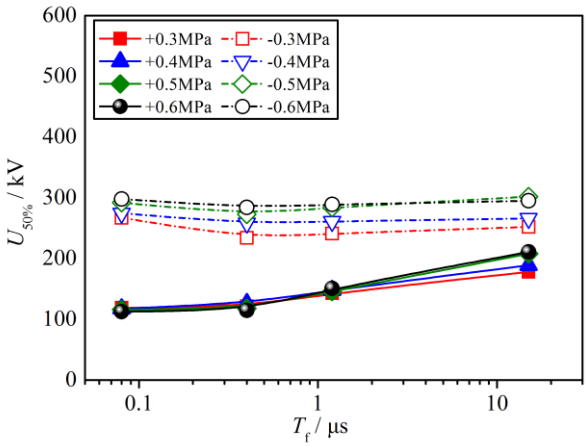

(b) L = 10 mm, D = 33 mm

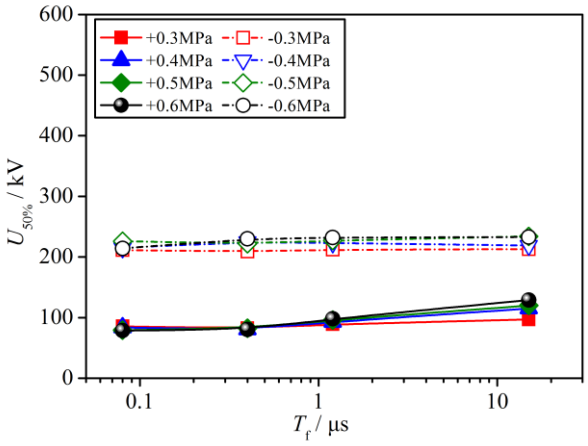

(c) L = 40 mm, D = 33 mm

Figure 5-7. 50% breakdown voltage vs. T_f for different needle length L

The U-shaped trend of the $U_{50\%}$-T_f curve for coaxial cylinder structure is not obvious. The discharge voltage decreases with the decrease of wavefront time and does not increase at short wavefront. It is because the shielding effect of the background electric field increases the discharge voltage and the critical volume of $E \geq E_{cr}$ near the needle electrode. The effective initial electron is easier to generate, then reducing the statistical delay of discharge. The effect of space charge on electric field

during discharge is stronger than the statistical delay on discharge voltage. So the discharge voltage is not significantly improved.

5.3 Discharge Characteristics of Coaxial Bus Structure System with Defects

5.3.1 Infunce of Wavefront Time on Discharge Voltage

Experiments based on the real defects, like a metal protrusion attached in the GIS bus have been conducted, as shown in Figure 5-8.

The results show a similar result that the 50% breakdown voltages increase with the increase of T_f. The wavefront time has a big influence on the insulation characteristics of GIS with a real defect. But there is a difference that the breakdown voltage at T_f = 0.08 μs is not high enough and the U-shaped trend is not obvious, which may be caused by electric field distribution due to background electric field and small radius of the needle tip.

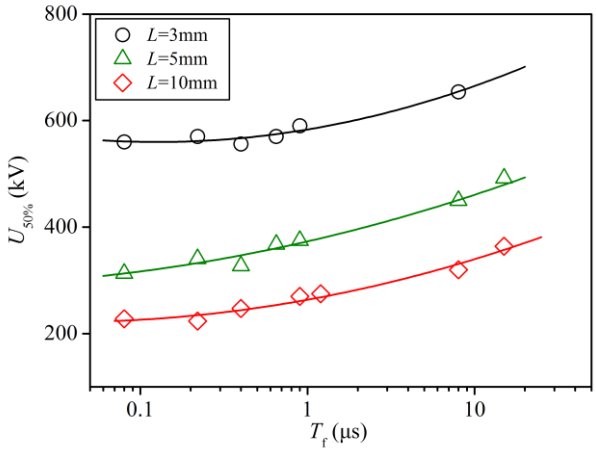

(a) 126 kV GIS, r = 0.5 mm

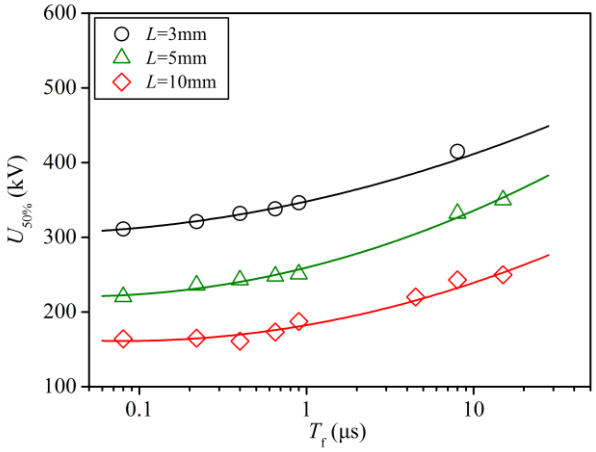

(b) 126 kV GIS, needle

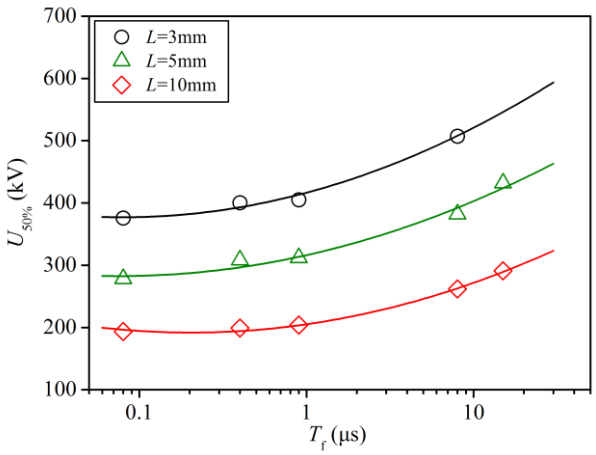

(c) 252 kV GIS, needle

Figure 5-8. 50% breakdown voltage vs. wavefront time for GIS with defects （p = 0.6 MPa）

5.3.2 Infunce of Wavefront Time on V-t Characteristic

Figure 5-9shows the V-t curves of three voltage-grade GIS when the needle defect length L = 10 mm. The point in the figure is the experimental value, and the solid line is the fitting curve obtained by using the fitting formula (4-1). Table 4-2 shows V-t curve fitting parameters at different gap distances. With the increase of gap distance, V-t curve U-shaped trend obviously. This is similar to the V-t characteristic of r = 0.5mm rod–plane gap as shown in Figure 5-3.

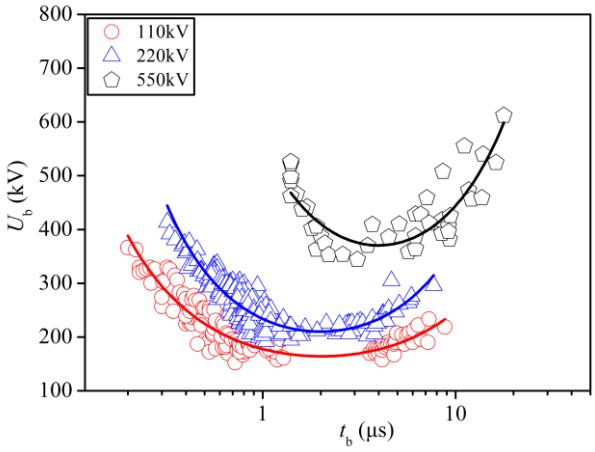

Figure 5-9 V-t curves for three voltage grade GIS with needle defects（L = 10 mm p = 0.6 MPa）

Table 5-2. The values of empirical constants for three voltage grade GIS

Voltage grade	a	b	c	2c
550 kV	2.74	-0.59	0.52	1.04
252 kV	2.36	-0.31	0.50	1.00
126 kV	2.25	-0.23	0.37	0.74

5.4 Brief Summary

1) The electrode structure has a great influence on the discharge characteristics. For

the GIS bus with a conductive protrusion, the shielding effect of the bus on the defect changes the electric field distribution of the gap, so that the $U_{50\%}$-T_f curves no longer show the U-shaped as the rod-plane electrode. The 50% discharge voltage of the bus with needle increases with wavefront time increase.

2) The field simulation results also show that with the increase of the needle length, the field nonuniformity factor increases. Therefore, when studying the discharge characteristics of GIS with defects, the shielding effect should be considered.

3) For coaxial bus structure system with defects, the 50% breakdown voltages increase with the increase of T_f.

CHAPTER 6. ON-SITE STANDARD LIGHTNING IMPULSE TEST TECHNOLOGY

The above research shows that the impulse voltage wavefront time has a great influence on the discharge characteristics of GIS with defects. The shorter the wavefront time is, the lower the breakdown voltage for the same defect is. On the other words, when using the impulse with steep wavefront has a higher probability to detect the defects, compared with the long wavefront impulse which used at current. Where conditions permit, the wavefront of the impulse voltage used in the on-site test should be as steep as possible. However, from the practical application, it is very difficult to generate impulses with wavefront time less than 1.2 μs for the large load capacitance. Therefore, compared with the long wave front oscillating impulse voltage currently used, the standard LI waveform is selected as the on-site impulse voltage test waveform, which is more effective for the detection of insulation defects in GIS. This chapter based on the compact low inductance Marx modular technology, developed a gas insulated impulse voltage generator for UHV GIS on-site LI test. And the technology has been carried out successfully in UHV substation.

6.1 The Bottleneck of Standard Lightning Impulse Test for Power Equipment with Large Capacity

With the increase of voltage grade, the capacitance of power equipment is large, especially for EHV and UHV GIS and long GIL equipment. The traditional impulse voltage test equipment, because of the large ontology inherent inductance, is hard to conduct standard LI test for equipment with large capacitance. The wavefront time (T_f) of LI is restricted by the circuit inductance and load capacitance [48]:

$$T_f = 4.66\sqrt{LC} \tag{6-1}$$

In particular, for the overall assembly equipment in the transformer substation, the capacitance is much larger. In addition, the installation and debugging workload of the traditional impulse voltage test equipment is huge in the field, so the on-site standard LI test has not been able to carry out. The reasons for the large inherent inductance of traditional open type impulse voltage generator are as follows:

(1) The insulating dielectric of traditional impulse voltage generator is air. So the enough insulation distance is needed, which makes the structure large. The larger the structure is, the higher the inherent inductance is.

(2) The wavefront resistances are distributed in every discharge units. Every wavefront resistance should have enough length for suffering the voltage of one discharge unit, which makes the total length of wavefront resistance longer and

the inductance of the discharging circuit increasing.

(3) The air spark switch has longer discharge channel, causing the inductance of the discharge circuit increasing.

(4) The capacitors have higher residual inductance.

The factors above make the traditional open type impulse voltage generator to have large inherent inductance (up to about 100μH). When the voltage grade is higher, the inherent inductance is larger. As a result, for testing a UHV-class GIS with capacitance up to about 3000pF, the front time T_f would exceed 2.2 μs, or even 3.0 μs in some cases, to generate a waveform with an overshoot rate β' of 10% or less using existing test facilities, as shown in in Figure 6-1 [28].

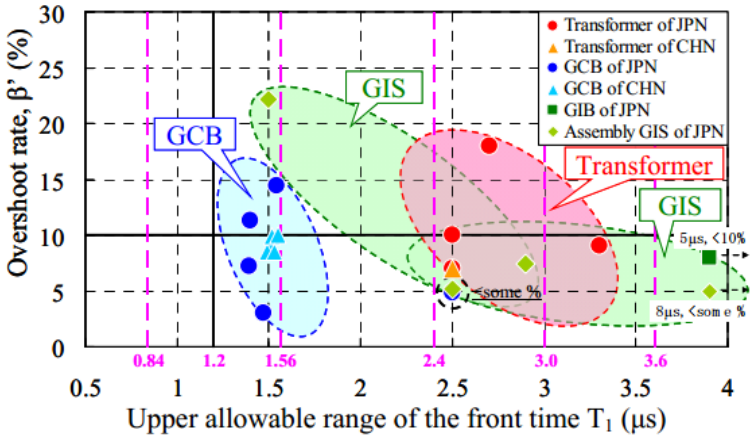

Figure. 6-1 T_f and β' in the actual LI voltage tests for UHV-class electric power equipment [28]

6.2 Development of a Compact Low Inductance Impulse Voltage Generator

As stated above, the on-site standard LI test for power equipment with large capacitance cannot be performed using a traditional impulse generator with large inductance (up to about 100 μH). Thus development of a compact low inductance impulse generator is essential.

Such a generator have been developed (Figure 6-2). The Marx generator is located within a fully enclosed pressure epoxy vessel filled with SF_6, typically to a pressure of 0.3 MPa. The generator consists of thirty 100 kV low-inductance capacitor groups and 15 gas spark switches. The main technical parameters of the generator are given in Table 6-1. The height of the generator is 7.6 m, much less than the height of the traditional impulse generator with the same rated voltage, typically 12 m. Thus the circuit inductance is lowered, and the maximum permissible capacitance of the equipment under test is increased.

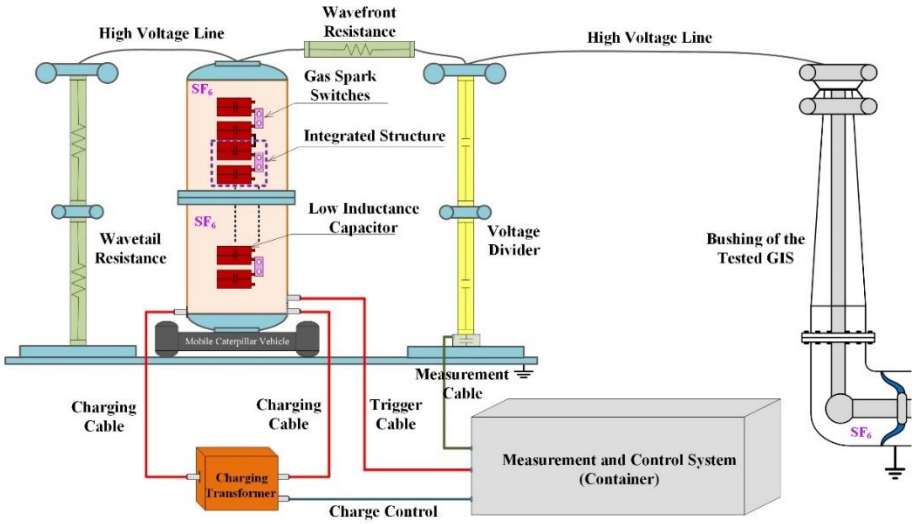

Figure 6-2. Structure of our compact low inductance impulse generator

Table 6-1. Main technical parameters of impulse generator

Item	Parameter
Insulating Medium	SF_6
Wave front Time	≥ 80 ns
Wavetail Time	10 ~ 2550 μs
Rated Voltage	3000 kV
Rated Capacity	300 kJ
Size	Height 7.6 m, Width 2.2 m
Weight	＜ 8 tonne

The generator has three important features, namely:

(a) a low inductance (< 50 nH) pulse capacitor,

(b) SF_6 gas insulating medium, facilitating a compact structure with a single-stage insulation distance only one-third of the corresponding distance in a conventional generator, and

(c) the design of the switch capacitor integration unit (Figure 6-3). Four low-inductance capacitors arranged in parallel meet the requirements of large capacity and low inductance. The capacitor group – gas spark switch – capacitor group integrated structure constitutes a 200 kV discharge unit, and fifteen such units are compactly arranged in series to constitute the 3000 kV Marx generator. The inductance of the single discharge unit is lower than 600 nH, approximately one-tenth of the inductance of the traditional open type impulse voltage generator.

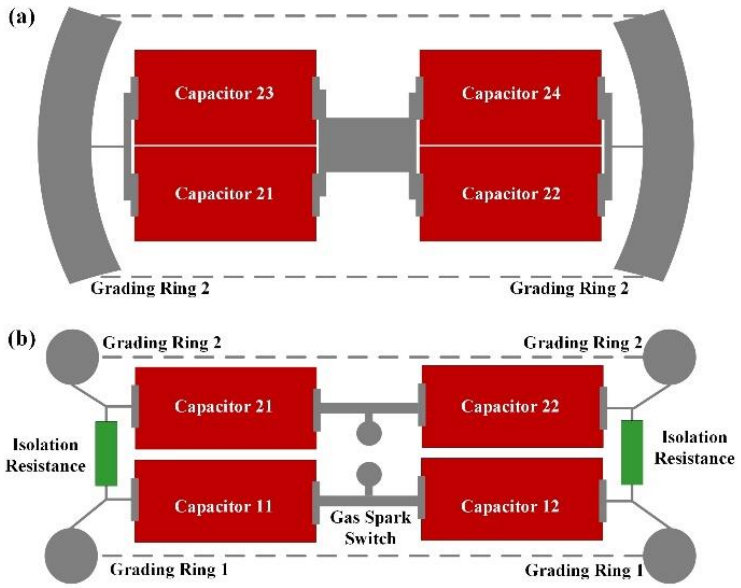

(a) a capacitor group (group 2); (b) a 200 kV discharge unit (unit 1).

Figure 6-3. Design of the switch capacitor integration unit

6.3 Application in UHV Substation

The on-site standard LI test for a 1100 kV GIS, using our low inductance impulse generator, was carried out in a UHV substation (Figure 6-4). This test is believed to have been the world's first on-site standard LI test for UHV GIS.

In order to guarantee an impulse voltage with short wavefront time T_f, one CB (circuit breaker) and its accessories were connected as the load for each test (shown in red in Figure 6-5). The test load could be connected / disconnected using the relevant disconnecting switches (DS) and earthing switches (ES); this substation adopts 3/2 CB connection. Impulses of both polarities and with amplitudes of 1705 kV, 1800 kV and 1920 kV were applied to the GIS. Figure 6-6 shows a typical test waveform under load conditions, measured by the voltage divider. The test waveforms, with different test loads, were double-exponential waveforms with front time in the range 1.52 ~ 2.28 μs, time to 50 % of the peak value in the range 48.9 - 59.4 μs, and an overshoot in the range 4.3 - 8.3 %. (Percentage overshoot = 100 (1 - (U_b/U_e)), where U_b and U_e are shown in Figure 6-6). The feature during the rise of the waveform (around -750 kV) was due to a discontinuity of the wave impedance Z associated with the high voltage wire, bushing, branch bus and CB, etc.

During the test, one insulation defect breakdown occurred under an 1800 kV positive impulse voltage. One discharge point on the bus and two discharge points on the inner wall of the cylinder were found (Figure 6-7). There a metal burr (one kind of insulation defect) may have been attached to the bus surface. It seems that, when the impulse was applied, a discharge originated on the bus surface and subsequently branched into two channels.

It is concluded that the on-site standard LI test, conducted using our low inductance impulse voltage generator, can detect defects in GIS equipment due to transportation

and/or installation more effectively than the non-standard LI test conducted using the traditional impulse generator.

Figure 6-4. UHV substation test site

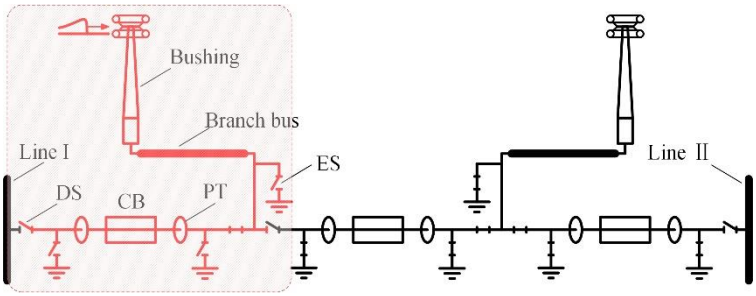

Figure 6-5. Schematic diagram of 3/2 CB connection and section test method

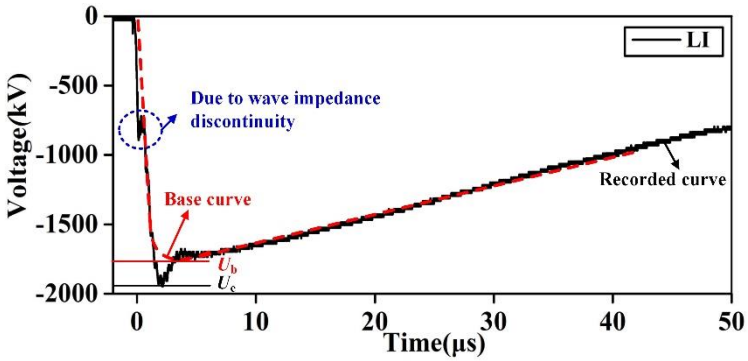

Figure 6-6. A typical test waveform

Figure 6-7. Location of discharges which occurred during testing

6.4 Brief Summary

1) A new fully enclosed and compact standard LI generator with low inductance has been developed, using SF_6 gas as the insulating medium and incorporating novel structural design of the switch capacitor integration unit.

2) Using the developed generator, an on-site standard LI test for 1100 kV GIS was successfully carried out in a UHV substation. One circuit breaker and its accessories were connected as the load for each test.

CHAPTER 7. CONCLUSIONS

1) The breakdown voltage for VFTO or standard LI in positive polarity is higher than that in negative polarity and the breakdown voltage of VFTO could be lower than that of standard LI at high gas pressure. The breakdown voltage of insulator under VFTO or standard LI in negative polarity is higher than that in positive polarity and the breakdown voltage of defective insulator under VFTO could be lower than that under LI by 8%. The 50% breakdown voltage vs. gas pressure shows the polarity reversion phenomenon, which can be explained by the migration and diffusion of space charges. The critical pressure of polarity reversion may increase with the increase of electric field inhomogeneity.

2) The impulse waveform parameters have little influence on the breakdown characteristics of a sound GIS system, but have significant influence on the breakdown characteristics of GIS system with defects. With the rise of gas pressure, the hump phenomenon occurs in the $U_{50\%}$-P curves. With the increase of impulse wave front time, the 50% breakdown voltages change significantly and the $U_{50\%}$-T_f curves tend to be U-shaped. The bigger the electric field factor f is, the more obvious the U-shaped trend is. The 50% breakdown voltages decrease significantly with the increase of impulse wave tail time. With the wave tail time increases, the discharge voltage gradually decreases, which could be explained by the area method.

3) The insulation defects detecting effectiveness of oscillating LI with long T_f around 10 μs is lower than that of standard LI. According to the voltage-time characteristic, it can be inferred that the T_f plays an important role in the insulation defect detecting effectiveness. With T_f increases, the 50% breakdown voltages for rod-plane gaps have an increased trend. The V-t curves of rod-plane gap under short T_f and long T_f present an opposite trend. The V-t curve shows a U-shaped in a wide range of t_b. The gap distance (or field nonuniformity factor) influences the shape of V-t curve. With the gap distance increase, the flat part of the curve and the mouth of the U-shaped V-t curve become narrower. The 50% flashover voltage of the insulator with surface conductive defects increases with the increase of wavefront time, which is similiar with the results of gas gap.

4) The effect of T_f is the effect of the slope of impulse dU/dt essentially. SF_6 gaps with a higher field nonuniformity factor f are more sensitive to dU/dt, also to T_f. Corona stabilization effect is not just in relationship with the rise rate of impulse, but also with electrode structure and gas pressure. The critical dU/dt for corona stabilization is calculated for different rod-plane gaps.

5) The electrode structure has a great influence on the discharge characteristics. For the GIS bus with a conductive protrusion, the shielding effect of the bus on the defect changes the electric field distribution of the gap, so that the $U_{50\%}$-T_f curves no longer

show the U-shaped as the rod-plane electrode. The 50% discharge voltage of the bus with needle increases with wavefront time increase. The field simulation results also show that with the increase of the needle length, the field nonuniformity factor increases.

6) A new fully enclosed and compact standard LI generator with low inductance has been developed, using SF_6 gas as the insulating medium and incorporating novel structural design of the switch capacitor integration unit. Using the developed generator, an on-site standard LI test for 1100 kV GIS was successfully carried out in a UHV substation. One circuit breaker and its accessories were connected as the load for each test.

ACKNOWLEDGEMENTS

I especially would like to express my sincerest gratitude to Professor Naoyuki Shimomura for giving me a chance to study as a Ph.D. student in his laboratory. As a foreign student, Professor Shimomura gives me lots of help not only in the research, but also in the daily life in Tokushima. He also gives me a chance and help in applying for the Power Academy fund. Thanks for the support of Power Academy.

I would like to express my acknowledgment to Associate Professor Kenji Teranishi, the students in our laboratory. They all are very frendly.

Also, I would like to extend my acknowledgement to Professor Toshihiro Moriga, Mrs. Asada, Doctor Yunong Wu, for their help in the abroad study affairs.

I would like to express my acknowledgment to Professor Masahide Hojo and Professor Masatake Kawada for their valuable advice and helpful suggestions.

Finally, I would like to extend my special acknowledgement to my father, mother and wife for their endless love, understanding, support, encouragement, patience and sacrifice throughout my study.

REFERENCES

[1] Y. Li, Y. Shang, L. Zhang, R. Shi and W. Shi, “Analysis of very fast transient overvoltages (VFTO) from onsite measurements on 800 kV GIS,” IEEE Trans. Dielectr. Electr. Insul., vol. 19, no. 6, pp. 2102–2126, 2012.

[2] K. Srivastava and M. Morcos, “A review of some critical aspects of insulation design of GIS/GIL systems,” in Proceedings of IEEE PES Transmission and Distribution Conference and Exposition, 2001, pp. 787–792.

[3] K. Tekletsadik and L. Campbell, “SF_6 breakdown in GIS,” in Proceedings of IEE on Science, Measurement and Technology, 1996, pp. 270–276.

[4] A. Sabot, A. Petit and J. Taillebois, “GIS insulation co-ordination: on-site tests and dielectric diagnostic techniques, A utility point of view,” IEEE Trans. Power Del., vol. 11, no. 3, pp. 1309–1316, 1996.

[5] J. Meppelink, K. Diederich, K. Feser, and W. Pfaff, “Very fast transients in GIS”, IEEE Trans. Power Del., vol. 4, pp. 223–233, 1989.

[6] U. Riechert and W. Holaus, “Ultra high-voltage gas-insulated switchgear-a technology milestone,” Eur. Trans. Electr. Power, vol. 22, no. 1, pp. 60–82, 2012.

[7] C. Li, J. He, J. Hu, R. Zeng and J. Yuan, “Switching transient of 1000-kV UHV system considering detailed substation structure,” IEEE Trans. Power Del., vol. 27, no. 1, pp. 112–122, 2012.

[8] D. Gu, P. Zhou, M. Dai, M. Xiu and H. He, “Overvoltages and insulation coordination of 1000-kV AC transmission systems in China,” Eur. Trans. Electr. Power, vol. 22, no. 1, pp. 83–93, 2012.

[9] W. Chen, X. Yan, S. Wang, C. Wang, Z. Li, M. Dai, C. Li, W. Liu, H. Chen, Q. Zhang, G. Wei, and M. Zhang, “Recent progress in investigation on very fast transient overvoltage in gas insulated switchgear,” Proc. CSEE, vol. 31, no. 31, pp. 1–11, 2011.

[10] H. Okubo and A. Beroual, “Recent trend and future perspectives in electrical insulation techniques in relation to sulfur hexafluoride (SF_6) substitutes for high voltage electric power equipment,” IEEE Electr. Insul. Mag., vol. 27, no. 2, pp. 34–42, 2011.

[11] U. Riechert, C. Neumann and H. Hama, “Very fast transient overvoltage (VFTO) in gas-insulated UHV substations,” presented at the CIGRE Advisory Group Report, Paris, France, 2010.

[12] S. Carsimamovic, Z. Bajramovic, M. Ljevak and M. Veledar, “Very fast electromagnetic transients in air insulated substations and gas insulated substations due to disconnector switching,” in Proceedings of International Symposium on Electromagnetic Compatibility, 2005, pp. 382–387.

[13] J. Amarnath, D. Paramahamsa, K. Narasimharao, B. Singh and K. Shrivastava, "Very fast transient over-voltages and transient enclosure voltages in gas insulated substations," in Proceedings of Annual Report Conference on Electrical Insulation and Dielectric Phenomena, 2003, pp. 506–509.

[14] S. Singha and M. Thomas, "Very fast transient overvoltages in GIS with compressed SF_6-N_2 gas mixtures," IEEE Trans. Dielectr. Electr. Insul., vol. 8, no. 4, pp. 658–664, 2001.

[15] Y. Yamagata, Y. Nakada, K. Nojima and M Kosakada, "Very fast transients in 1000 kV gas insulated switchgear," in Proceedings of IEEE Transmission and Distribution Conference, 1999, pp. 501–508.

[16] A. Cookson, "Review of high voltage gas breakdown and flashover of insulators in compressed sulfur hexafluoride," in Proceedings of 3rd International Conference on Properties and Applications of Dielectric Materials,1991, pp. 369–376.

[17] A. Pedersen, "On the electrical breakdown of gaseous dielectrics-an engineering approach," IEEE Trans. Dielectr. Electr. Insul., vol. 24, no. 5, pp. 721–739, 1989.

[18] J. Laghari and A. Qureshi, "A review of particle-contaminated gas breakdown," IEEE Trans. Dielectr. Electr. Insul., vol. EI-16, no. 5, pp. 388–398, 1981.

[19] Q. Zhang, J. Jia, L. Yang, F. Tao, and Y. Qiu, "Mechanism of discharge development in SF_6 with and without spacers under fast oscillating impulse condition," Journal of Applied Physics, vol. 98, pp. 103301(1)–103301(5), Nov. 2005.

[20] J. Meppelink, K. Diederich, K. Feser, and W. Pfaff, "Very fast transients in GIS," IEEE Transactions on Power Delivery, vol. 4, pp. 223–233, Jan. 1989.

[21] Y. Yamagata, Y. Nakada, K. Nojima, M. Kosakada, J. Ozawa, and I. Ishigaki, "Very fast transients in 1000 kV gas insulated switchgear," in IEEE Transmission and Distribution Conference, 1999, pp. 501–508.

[22] CIGRE Working Group 33/23.12, "Insulation co-ordination of GIS: questions on the influence of on-site tests and dielectric diagnostics," 1992.

[23] P. Sporn, "Rationalization of Transmission Insulation Strength-II" Need for, Present Status, and Necessary Developments for Carrying Through", AIEE, Trans., Vol. 49, pp. 1470-1477, 1930.

[24] S. Okabe, J. Takami, T. Tsuboi, G. Ueta, A. Ametani and K. Hidaka, "Discussion on standard waveform in the lightning impulse voltage test", IEEE Trans. Dielectr. Electr. Insul., Vol. 20, No. 1, pp. 147-156, 2013.

[25] High-Voltage Test Techniques Part 1: General Defiitions and Test Requirements, IEC Standard 60060-1, 2010-09-29.

[26] Insulator and Lightning Subcommittee of the Transmission committee, "Recommendations for Impulse Voltage Testing", AIEE, Trans., Vol. 52, pp. 466-471, 1933.

[27] High voltage switchgear and controlgear-Gas-insulated metal enclosed switchgear, IEC Standard 62271-203, 2003-11.

[28] Okabe S, Ueta G, Tsuboi T, et al. Study on Lightning Impulse Test Waveform for UHV-class Electric Power Equipment[J]. IEEE transactions on dielectrics and electrical insulation, 2012, 19 (3): 803-811.

[29] Kuffel E, Yializis A, "Impulse breakdown of positive and negative rod-plane gaps in SF_6-N_2 mixtures," IEEE Transactions on Power Apparatus and systems, 1978, (6): 2359-2366.

[30] Li J, Zhang L, Hu D, et al, "Breakdown characteristics of SF_6 in quasi-uniform field under oscillating lightning impulse voltages," IEEE transactions on dielectrics and electrical insulation, 2017, 24 (2): 915-922.

[31] Okabe S, Tsuboi T, Ueta G, et al, "Basic study of fitting method for base curve extraction in lightning impulse test techniques," IEEE transactions on dielectrics and electrical insulation, 2010, 17 (1).

[32] Okabe S, Yuasa S, Kaneko S, et al, "Evaluation of breakdown characteristics of gas insulated switchgears for non-standard lightning impulse waveforms-method for converting non-standard lightning impulse waveforms into standard lightning impulse waveforms," IEEE transactions on dielectrics and electrical insulation, 2009, 16 (1): 42-51.

[33] Wiegart N, Niemeyer L, Pinnekamp F, et al, "Inhomogeneous field breakdown in GIS-the prediction of breakdown probabilities and voltages. II. Ion density and statistical time lag," IEEE transactions on power delivery, 1988, 3 (3): 931-938.

[34] Yoshida T, Fujinami H, Kawamoto T, "V-t characteristics of SF_6 gas during lightning surges," Electrical engineering in Japan, 1997, 119 (4): 1-11.

[35] Luxa G, "Recent Research Activity on the Dielectric Performance of SF_6 with Special Reference to Very Fast Transients," CIGRE, 1988.

[36] Matsumoto S, Aoyagi H, Murase H, et al, "Non-Uniform Field Flashover Characteristics in SF_6 Gas under Very Fast Transient Overvoltages," IEEJ Transactions on Power and Energy, 1990, 126 (9): 769-777.

[37] Ueta G, Kaneko S, Okabe S, "Evaluation of breakdown characteristics of gas insulated switchgears for non-standard lightning impulse waveforms-breakdown characteristics for double-frequency oscillations under non-uniform electric field," IEEE Transactions on Dielectrics and Electrical Insulation, 2009, 16 (3): 815-825.

[38] Qiaogen ZHANG, "Discharge characteristics of SF_6 gas gap and insulator surface," Doctoral dissertation, Xi'an Jiaotong University, 1996.

[39] F. Pinnekamp and L. Niemeyer, "Qualitative model of breakdown in SF_6 in inhomogeneous gaps," Journal of Physics D: Applied Physics, vol. 16, no. 7, p. 1293, 1983.

[40] B. Mazurek, J. Cross, and R. Heeswijk, "The effect of a metallic particle near a spacer on flashover phenomena in SF_6," IEEE Transactions on Electric Insulator, vol. 28, no. 2, pp. 219–229, 1993.

[41] F. Wang, Y. Qiu, W. Pfeiffer, and E. Kuffel, "Insulator surface charge accumulation under impulse voltage," IEEE Transactions on DielectrIcs and Electric Insulation, vol. 11, no. 5, pp. 847–854, 2004.

[42] M. Li and A. Vlastos, "Influence of impulse voltage waveshape on the flashover of clean and particle-contaminated spacers in SF_6 gas-insulated system," IEEE Transactions on Power Delivery, vol. 4, no. 1, pp. 326–334, 1989.

[43] O. Yamamoto, T. Hara, and T. Takuma, "The role of leader re-illumination in the development of surface discharges in SF_6 exposed to a very fast transient overvoltage," Journal of Physics D: Applied Physics, vol. 31, pp. 2997–3003, 1998.

[44] Q. Zhang, F. Tao, Z. Li, W. Ding, and A. Qiu, "Effect of pulse front time on the glow discharge in nonuniform electric field," IEEE Transactions on Plasma Science, vol. 36, no. 4, pp. 1008–1009, 2008.

[45] S. Okabe, S. Yuasa, S. Kaneko, and G. Ueta, "Evaluation of breakdown characteristics of gas insulated switchgears for non-standard lightning impulse-Breakdown characteristics for non-standard lightning impulse waveforms under diverse conditions," IEEE Trans. Dielectr. Electr. Insul., Vol. 15, pp. 1415-1423, 2008.

[46] B. Lee, Y. Baek, H. Choi, and S. Oh, "Impulse breakdown characteristics of the plane-to-plane electrode system with a needle-shaped protrusion in SF_6," Curr. Appl. Phys., Vol. 7, pp. 289-295, 2007.

[47] X. Qiu, I. Chalmers, and Y. Qiu, "Effect of initiatory electrons on breakdown characteristics of SF_6 and its mixtures," Proc. of IEE Sci. Meas. Technol., Vol. 148, pp. 80-83, 2001.

[48] T. Wen, Q. Zhang, C. Guo, et al, "3-MV Compact very fast transient overvoltage generator for testing ultra-high-voltage gas-insulated switchgear," Electr. Insul. Mag., Vol. 30, No. 6, pp. 26-33, 2014.

[49] L. Zhang, Q. Zhang, S. Liu, F. Liu, L. Li, Y. Yin, W. Shi and W. Chen, "Breakdown characteristics of 1100 kV GIS under very fast transient overvoltage and lightning impulse," IEEE Trans. Dielectr. Electr. Insul., Vol. 19, No. 3, pp. 1029-1036, 2012.

[50] H. Shinkai, H. Goshima, M. Yashima, et al, "Quantitative evaluation of lightning surge range voltage–time characteristics in high-pressure SF_6 gas," Electr. Eng. Jpn., Vol. 159, No. 4, pp. 8-17, 2007.

[51] K. Stankovic, P. Osmokrovic, C. Dolicanin, et al, "Time enlargement law for gas pulse breakdown," Plasma Sources Sci. Technol., Vol. 18, No. 2, pp. 25-28, 2009.

[52] G. Carrara and L. Thione, "Switching surge strength of large air gaps: a physical approach", IEEE Trans. Power App. Syst., Vol. 95, No. 2, pp. 512-524, 1976.

[53] C. Gu, W. Zhang, J. Fan, Z. Su, X. Wang, W. Liao and Q. Li, "Influence of rod electrode structure on switching impulse discharge characteristics of rod-plane air

gap", Proc. Chinese Soc. Electr. Eng. (CSEE), Vol. 31, No. 28, pp. 120-127, 2011.

[54] Guide for Withstand Voltage and Insulated Test of Gas-insulated Metal-enclosure Switchgear on sit, DL/T 555, 2004.

[55] Berg D, Works C, "Infunce of space charge on electric breakdown of sulfur hexafluoride in nonuniform fields," Transactions of the American Institute of Electrical Engineers Part III: Power Apparatus and Systems, 1958, 77 (3): 820-823.

[56] Gas-insulated Metal-enclosed Switchgear for Rated Voltages of 72.5 kV and above, GB/T 7674, 2008.

[57] Q. Zhang, L. Yang, Q. Chen, et al. The effect of impulse rising steepness on streamer to leader transition in non-uniform field gap in SF_6[J]. J. Appl. Phys. D: Applied Physics, 2003, 36 (10): 1212.

[58] N.H. Malik and A.H. Qureshi, "Breakdown gradients in SF_6-N_2, SF_6-Air and SF_6-CO_2 Mixtures", IEEE Trans. Electr. Insul., vol. 15, pp. 413-418, 1980.

[59] T.W. Dakin, G. Luxa, G. Oppermann, J. Vigreux, G. Wind, H. Winkelkemper, "Breakdown of Gases in Uniform Fields", Electra, No 32, pp. 61-82, 1974

[60] T. Hinterholzer, W. Thomas and W. Boeck, "The influence of space-charge on the breakdown in SF_6", Gaseous Dielectrics IX, Springer US, pp. 383-389, 2001.

LIST OF PUBLICATIONS

Journals/Transactions:

1) “On-site Standard Lightning Impulse Test for 1,100-kV Gas-Insulated Switchgear with Large Capacitance”

Tao Wen, Qiaogen Zhang, Yifan Qin, Junping Zhao, Jingtan Ma, and Zhicheng Wu, ***Naoyuki Shimomura***, Fengbo Tao and Yongyong Jia, Yu Yin, Weidong Shi, Weijiang Chen

IEEE Electrical Insulation Magazine, Vol. 32, No. 6, Page 36-43, November, 2016, Published.

2) “Discussion on Lightning Impulse Test Waveform According to Breakdown Characteristics of SF_6 Gas Gaps”

Tao Wen, Qiaogen Zhang, Lingli Zhang, Jingtan Ma, Can Guo, Ming Chen, Yuan Li, ***Naoyuki Shimomura***, Weijiang Chen

IEEE Transactions on Dielectrics and Electrical Insulation, Vol. 24, No. 4, Page 2306~2313, August, 2017, Published.

3) “Research on the Detecting Effectiveness of On-site Lightning Impulse Test for GIS Equipment with Insulation Defects”

Tao Wen, Qiaogen Zhang, Jingtan Ma, Xuandong Liu, Zhicheng Wu, Lingli Zhang, Junping Zhao, ***Naoyuki Shimomura***, Weijiang Chen

IEEE Transactions on Dielectrics and Electrical Insulation, Vol. 25, No. 2, Page 551~558, April, 2018, Published.

International Conferences:

1) “Research on Impulse Withstand Test Effectiveness from Insulation Characteristics of SF_6 at Highly Inhomogeneous Electric Field”

Tao Wen, Qiaogen Zhang, Lingli Zhang, Jiangtan Ma, Min Chen, ***Naoyuki Shimomura***, Zhibing Li

IEEE 1st International Conference on Electrical Materials and Power Equipment, Xi’an, China, Page 482~485, May, 2017, Published.

2) “Research on Shielding Effect of Background Electric Field for GIS Bus with a Conductive Protrusion Under Impulses”

Tao Wen, Qiaogen Zhang, Ming Chen, Jiangtan Ma, Zhicheng Wu, ***Naoyuki Shimomura***, Yu Yin, Weijiang Chen

IEEE 12th International Conference on the Properties and Applications of Dielectric

Materials, Xi'an, China, May 20th ~ 24th, 2018, Published.

Domestic Conferences:

1) "Research on Insulation Defect Detection Effectiveness of On-site Impulse Voltage Test for GIS Equipment"

Tao Wen, ***Naoyuki Shimomura***, Kenji Teranishi, Qiaogen Zhang

平成 29 年電気学会全国大会，平成 29 年 3 月 15 日～17 日，富山大学，7-078: 19.